

Einstein Probe Discovery of EP J182730.0-095633: A New Black Hole X-ray Binary Candidate in Faint Outburst?

H. Q. CHENG¹, Q. C. ZHAO^{1,2,3}, L. TAO¹, H. FENG¹, F. COTI ZELATI^{4,5}, H. W. PAN¹, A. L. WANG², Y. N. WANG¹, M. Y. GE², A. RAU⁶, A. MARINO^{4,5}, L. ZHANG², W. J. ZHANG¹, F. CAROTENUTO⁷, L. JI⁸, C. C. JIN^{1,3,9}, D. Y. LI¹, B. F. LIU^{1,3}, Y. LIU¹, E. L. QIAO^{1,3}, N. REA^{4,5}, R. SORIA^{10,11}, S. WANG¹, Z. YAN¹², W. YUAN^{1,3}, B. ZHANG^{13,14}, G. B. ZHANG^{15,16}, S. N. ZHANG^{2,3}, W. D. ZHANG¹, A. BEARDMORE¹⁷, J. S. BRIGHT¹⁸, X. L. CHEN¹⁹, Z. FAN^{1,3}, S. Y. FU¹, J. P. U. FYNBO^{20,21}, J. W. HU¹, J. J. JIN¹, P. G. JONKER²², A. K. H. KONG²³, E. KUULKERS²⁴, C. K. LI², H. L. LI¹, Z. K. LIN¹, C. X. LIU¹⁹, H.-Y. LIU¹, J. Z. LIU^{25,3}, X. W. LIU¹⁹, Z. LU^{26,27}, C. MAITRA⁶, H. Y. MU¹, C.-Y. NG²⁸, Y. L. QIU¹, S. TINYANONT²⁹, Y. WANG³⁰, S. X. WEN¹, S. S. WENG³¹, JIANFENG WU³², D. XU¹, Y. K. YAN²⁶, Z. YAN¹⁵, Y.-P. YANG¹⁹, P. ZHANG^{26,27}, S. ZHANG², Q. ZHAO¹, Z. M. CAI³³, Y. CHEN², Y. F. CHEN³⁴, C. Z. CUI^{1,3}, W. W. CUI², H. B. HU¹, M. H. HUANG^{1,3}, S. M. JIA², G. JIN³⁵, Z. X. LING^{1,3,9}, H. Q. LIU³³, S. L. SUN³⁴, X. J. SUN³⁴, Y. F. XU^{1,3}, C. ZHANG^{1,3}, M. ZHANG¹ AND Y. H. ZHANG³³

¹National Astronomical Observatories, Chinese Academy of Sciences, 20A Datun Road, Beijing 100101, China

²Key Laboratory of Particle Astrophysics, Institute of High Energy Physics, Chinese Academy of Sciences, Beijing 100049, China

³School of Astronomy and Space Science, University of Chinese Academy of Sciences, 19A Yuquan Road, Beijing 100049, China

⁴Institute of Space Sciences (ICE), CSIC, Campus UAB, Barcelona, E-08193, Spain

⁵Institut d'Estudis Espacials de Catalunya (IEEC), Barcelona, E-08034, Spain

⁶Max Planck Institute for Extraterrestrial Physics, Garching, 85748, Germany

⁷INAF-Osservatorio Astronomico di Roma, Via Frascati 33, I-00078, Monte Porzio Catone (RM), Italy

⁸School of Physics and Astronomy, Sun Yat-Sen University, Zhuhai 519082, China

⁹Institute for Frontier in Astronomy and Astrophysics, Beijing Normal University, Beijing 102206, China

¹⁰INAF – Osservatorio Astrofisico di Torino, Pino Torinese, I-10025, Italy

¹¹Sydney Institute for Astronomy, School of Physics A28, The University of Sydney, NSW 2006, Australia

¹²Shanghai Astronomical Observatory, Chinese Academy of Sciences, 80 Nandan Road, Shanghai, 200030, China

¹³Nevada Center for Astrophysics, University of Nevada Las Vegas, NV 89154, USA

¹⁴Department of Physics and Astronomy, University of Nevada Las Vegas, NV 89154, USA

¹⁵Yunnan Observatories, Chinese Academy of Sciences, Kunming 650216, China

¹⁶Key Laboratory for the Structure and Evolution of Celestial Objects, Chinese Academy of Sciences, Kunming 650216, China

¹⁷School of Physics and Astronomy, University of Leicester, University Road, Leicester, LE1 7RH, UK

¹⁸Astrophysics, Department of Physics, University of Oxford, Keble Road, Oxford OX1 3RH, UK

¹⁹South-Western Institute for Astronomy Research, Yunnan University, Kunming, Yunnan 650504, China

²⁰Cosmic Dawn Center (DAWN)

²¹Niels Bohr Institute, University of Copenhagen, Jagtvej 128, 2200, Copenhagen N, Denmark

²²Department of Astrophysics/IMAPP, Radboud University, P.O. Box 9010, 6500 GL, Nijmegen, The Netherlands

²³Institute for Cosmic Ray Research, The University of Tokyo, Kashiwa City, Chiba 277-8582, Japan

²⁴ESA/ESTEC, Noordwijk, 2201 AZ, the Netherlands

²⁵Xinjiang Astronomical Observatory, Chinese Academy of Sciences, Urumqi 830011, China

²⁶College of Mathematics and Physics, China Three Gorges University, Yichang 443002, China

²⁷Center for Astronomy and Space Sciences, China Three Gorges University, Yichang 443002, China

²⁸Department of Physics, University of Hong Kong, Pokfulam Road, Hong Kong, China

²⁹National Astronomical Research Institute of Thailand, 260 Moo 4, Donkaew, Maerim, Chiang Mai, 50180, Thailand

³⁰Key Laboratory of Dark Matter and Space Astronomy, Purple Mountain Observatory, Chinese Academy of Sciences, Nanjing 210023, China

³¹Department of Physics and Institute of Theoretical Physics, Nanjing Normal University, Nanjing, China

³²Department of Astronomy, Xiamen University, Xiamen, Fujian 361005, China

³³Innovation Academy for Microsatellites, Chinese Academy of Sciences, Shanghai 201210, China

³⁴Shanghai Institute of Technical Physics, Chinese Academy of Sciences, Shanghai 200083, China

Corresponding author: L. Tao

taolian@ihep.ac.cn

³⁵*North Night Vision Technology Co., LTD, Nanjing, China*

(Received; Revised; Accepted)

Submitted to ApJL

ABSTRACT

Black hole X-ray binaries (candidates) currently identified in our galaxy are mainly transient sources, with the majority discovered through the detection of their X-ray outbursts. Among these, only four were found during faint outbursts exhibiting peak X-ray luminosities $L_X \lesssim 10^{36}$ erg s⁻¹, likely due to the previous lack of sensitive, wide-field monitoring instruments in the X-ray band. In this *Letter*, we present the discovery of an intriguing X-ray transient, EP J182730.0-095633, via the *Einstein Probe* (EP) and subsequent multi-wavelength follow-up studies. This transient, located on the Galactic plane, experienced a faint and brief X-ray outburst lasting about 20 days. Its X-ray spectrum is non-thermal and consistent with a power-law model with a nearly constant photon index of $\Gamma \sim 2$ throughout the outburst. A long-lasting millihertz quasi-periodic oscillation (QPO) signal was detected in its X-ray light curve, centered around a frequency of ~ 0.04 Hz. A transient near-infrared source was identified as its counterpart, although no optical emission was detectable, likely due to significant extinction. A radio counterpart was also observed, displaying an inverted radio spectrum with $\alpha \sim 0.45$. The X-ray spectral and temporal characteristics, along with the multi-wavelength properties, indicate that the source is a faint low-mass X-ray binary, with the compact object likely being a black hole. This work demonstrates the potential of the EP in discovering new X-ray binaries by capturing faint-level X-ray outbursts.

Keywords: Transient sources – X-rays: binaries – Black holes – X-rays: individual (EP J182730.0-095633)

1. INTRODUCTION

Black holes (BHs) are among the most mysterious celestial objects in the universe. They provide a unique laboratory for studying the General Relativity effects and other physical processes in strong gravitational fields. As the inevitable evolutionary destiny and remnant of massive stars, stellar-mass BHs, with masses in the typical range of several to several tens of solar masses, are of great importance in understanding the formation and growth of BHs, as well as the evolution of massive stars. So far, stellar-mass BHs have been found to exist in binary systems termed X-ray binaries (XRBs, e.g. van Paradijs 1995; Lewin et al. 1995; Remillard & McClintock 2006). In our galaxy, they have preferably been found in binary systems with a low-mass companion star, termed Low-Mass X-ray Binaries (LMXBs, see Kalemci et al. 2022; Bahramian & Degenaar 2023, for detailed reviews). LMXBs are mostly X-ray transient sources, exhibiting bright, sporadic outbursts that typically last from months to years (e.g. Remillard & McClintock 2006; Belloni et al. 2011).

Currently, over 70 transient BH (candidate) X-ray binaries have been identified¹. Among these, about 20 contain a compact object confirmed to be in the BH mass range using dynamical methods, i.e., by measuring the orbital motion of their companion stars (Corral-Santana et al. 2016; Avakyan

et al. 2023). Historically, these systems were predominantly discovered via capturing their transient outbursts by a series of wide-field X-ray monitoring instruments that have been flown since the 1970's, such as the *Ariel-V* (Villa et al. 1976), the all-sky monitor WATCH on board Granat satellite (Brandt et al. 1990), the All-Sky Monitor (ASM) on board *Rossi X-ray Timing Explorer* (RXTE; Levine et al. 1996), the INTErnational Gamma-Ray Astrophysics Laboratory (INTEGRAL; Winkler et al. 2003; Kuulkers et al. 2021), the Burst Alert Telescope (BAT; Barthelmy et al. 2005) on board the *Neil Gehrels Swift Observatory* (Swift; Gehrels et al. 2004), and the Monitor of All-sky X-ray Image (MAXI; Matsuoka et al. 2009). For the vast majority of these systems, the detected X-ray outbursts reached a peak luminosity typically over 10^{37} erg s⁻¹ (e.g. Yan & Yu 2015; Tetarenko et al. 2016), making them bright enough to be detected by most of the X-ray monitors mentioned above.

Only four BHs (candidates) were discovered by the detection of their X-ray emission during faint outbursts, with a peak luminosity $L_X \lesssim 10^{36}$ erg s⁻¹ (Wijnands et al. 2006), namely, Swift J1357.2-0933 (Corral-Santana et al. 2013), XTE J1118+480 (Wagner et al. 2001), XTE J1728-295 (Swank & Markwardt 2001; Walter et al. 2004), and CX-OGC J174540.0-290031 (Muno et al. 2005a; Porquet et al. 2005). The first two systems were confirmed to harbor a black hole through dynamical mass measurements, while the latter two were well consistent with BH transients in their observed properties. The small number of BHs found during

¹ <https://www.astro.puc.cl/BlackCAT/transients.php>

faint outbursts can be explained in the sense that the peak X-ray brightness of the majority of such systems fall below the sensitivity of the past and most current wide-field monitors, while the sensitive X-ray telescopes (such as *Chandra* and *XMM-Newton*) have too small field of view (FoV) to catch the outbursts in real time (the case of CXOGC J174540.0-290031 is an exception and the chance of such detections is expected to be low).

It has long been recognized that the number of black hole X-ray binaries (BHXRBS) known so far is much smaller than what was hypothesized to exist in our galaxy (van den Heuvel 1992). Based on the distances and spatial distributions of the known BHXRBS, it was estimated that there are more than 10^3 BHXRBS in our galaxy (Corral-Santana et al. 2016). In fact, stellar evolution models predicted that there could be as many as $10^8 - 10^9$ BHs lurking in our galaxy (e.g. Brown & Bethe 1994; Timmes et al. 1996; Meier 2012). This ‘missing’ population of stellar-mass BHs has been a topic of extensive debate for decades (Hailey et al. 2018). The apparently very low detectability of BHXRBS is likely attributable to their presumably transient nature and the fact that most of their outbursts are likely too faint to be detectable by the past and most of the current X-ray wide-field monitors. It is thus expected that, with the advent of X-ray wide-field monitors having significantly improved sensitivity, more of such systems could be revealed. Nonetheless, further challenges lie with the identification of the nature of the compact object (be it a BH or a neutron star) for LMXBs, which requires dense monitoring and prompt multi-wavelength follow-up observations (Wijnands et al. 2006; Bahramian & Degenaar 2023).

The *Einstein Probe* (EP; Yuan et al. 2022), launched on January 9th 2024, carries the Wide-field X-ray Telescope (WXT)—a wide-field monitor with a FoV of ~ 3800 square degrees built from lobster-eye micro-pore optics. Operating in the 0.5–4 keV band, WXT can reach a sensitivity of ~ 1 mCrab ($\sim (2 - 3) \times 10^{-11}$ erg s $^{-1}$ cm $^{-2}$ in 0.5–4 keV) at an exposure of ~ 1000 s, which is several-tens times more sensitive than the other currently operating wide-field monitors. For BHXRBS within our galaxy, an X-ray outburst brighter than $\sim 10^{35}$ erg s $^{-1}$ will likely be detected by WXT within $\sim 10^3$ s, enabling the detection of outbursts that are ~ 100 times fainter than those previously detectable. The other instrument on board EP is the Follow-up X-ray Telescope (FXT, Chen et al. 2020) operating in 0.3–10 keV band, which provides source localization of $5 - 10''$ and sensitivity of $\sim 10^{-14}$ erg s $^{-1}$ cm $^{-2}$ at an exposure of 10^4 s. It is expected that EP will detect new BHXRBS systems, particularly those undergoing faint, short-lived outbursts (Yuan et al. 2025).

In this *Letter*, we report on the discovery and multi-wavelength follow-up observations of an X-ray transient EP J182730.0-095633 (EP240904a, Cheng et al. 2024b) located

on the Galactic plane. The spectral, temporal, and multi-wavelength properties observed favor this source being a new BHXRBS candidate experiencing a faint outburst lasting for about 20 days. This paper is organized as follows: in Section 2, we describe the observations and data reduction procedures. The results are presented in Section 3 and discussed in Section 4. The conclusion is given in Section 5.

2. OBSERVATIONS AND DATA REDUCTION

2.1. X-ray

EP J182730.0-095633 was first detected as an X-ray transient (designated EP240904a) in an observation starting on September 4th, 2024, at 10:12:56 UT by EP/WXT (Cheng et al. 2024b). The source was not detected during a WXT observation taken one day before (Figure 1). Following the detection of the source, a series of follow-up observations were carried out with EP/FXT starting on September 6th, 2024 and lasting until September 24th. These observations provided a more precise source position at R.A. (J2000.0) = $18^{\text{h}}27^{\text{m}}30.0^{\text{s}}$ and Decl. (J2000.0) = $-9^{\circ}56'33''$, with an uncertainty of $10''$ at the 90% confidence level (Cheng et al. 2024b). Meanwhile, several other X-ray telescopes were triggered and joined the follow-up campaign, including the *Swift*, the *Neutron Star Interior Composition Explorer* (NICER; Gendreau et al. 2016), the *Nuclear Spectroscopic Telescope Array* (NuSTAR; Harrison et al. 2013), and the *Hard X-ray Modulation Telescope* (*Insight*-HXMT; Zhang et al. 2020)². The X-ray Telescope (XRT) aboard *Swift* provided an enhanced positional accuracy (Evans et al. 2009, 2020), by applying a correction based on the photometry provided by the Ultra-Violet/Optical Telescope (UVOT): R.A. (J2000.0) = $18^{\text{h}}27^{\text{m}}30.1^{\text{s}}$ and Decl. (J2000.0) = $-9^{\circ}56'41.4''$, with an uncertainty of $2.1''$ at the 90% confidence level. For this work, we adopt the *Swift*/XRT coordinates as the X-ray position of EP J182730.0-095633. It is important to point out that EP J182730.0-095633 resides on the Galactic plane ($l = 21.3634^{\circ}$, $b = 0.7244^{\circ}$), suggesting a likely Galactic origin for this transient. The observation log is summarized in Table B.1, and the data reduction process is detailed in Section A.1.

2.2. Optical and infrared

Follow-up observations of EP J182730.0-095633 were carried out in the optical and near-infrared bands with various ground- and space-based telescopes. These include the Thai Robotic Telescope (TRT), the Nordic Optical Telescope (NOT), the Altay 1-Meter Telescope (ALT100C), the Visible Telescope on board the *Space-based multi-band astronomical Variable Objects Monitor* (SVOM/VT), the

² Due to contamination from nearby sources, data from *Insight*-HXMT were excluded from further analysis.

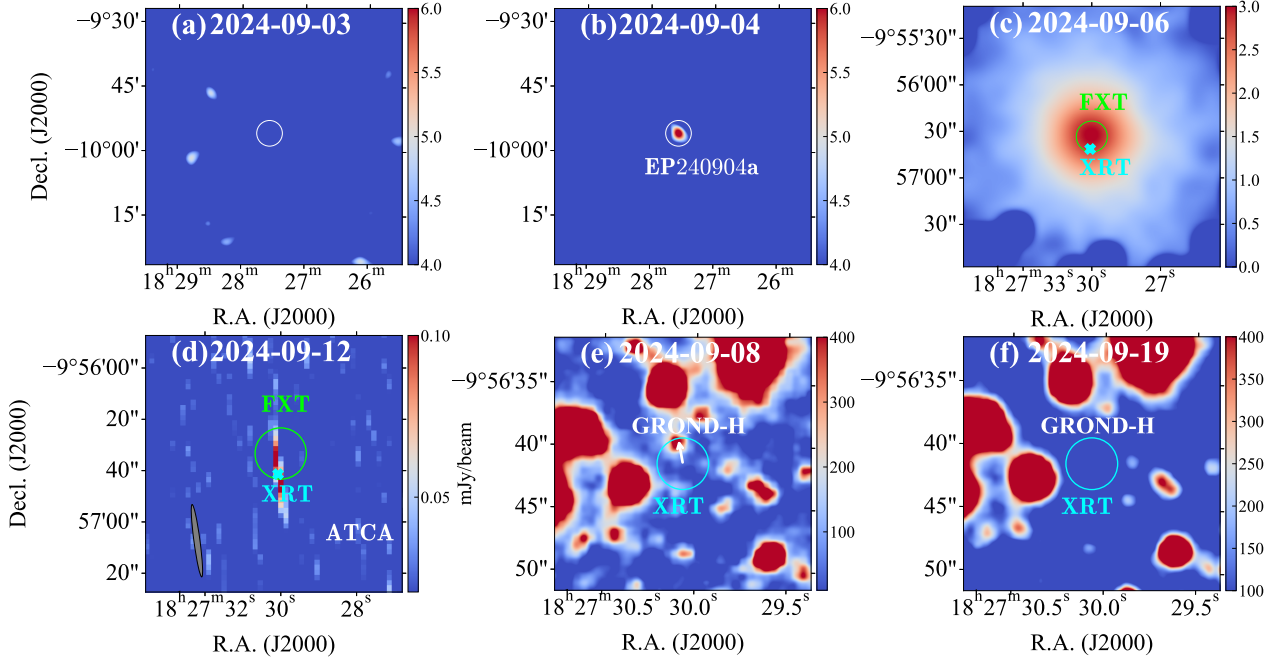


Figure 1. Panels (a) and (b) show *EP/WXT* images of EP J182730.0-095633 from September 3rd to 4th, 2024 (ObsIDs are 06800000068 and 06800000067, respectively). Panel (c) presents *EP/FXT* module A (FXTA) image obtained with Full Frame (FF) mode on September 6th, 2024. Panel (d) displays *ATCA* (5.5 GHz) images on September 12th, 2024. The restoring beam ($19.5'' \times 1.2''$, 5.5°) is indicated as a gray elliptical shape in the bottom left corner. Panels (e) and (f) show near-infrared (*H* bands) images obtained from GROND on September 8th and 19th, 2024, respectively. The potential NIR counterpart is denoted by the white arrow in Panel (e). The white, green, and cyan circles represent the positional errors of WXT, FXT, and XRT, respectively.

Tsinghua-NAOC Telescope (TNT, Huang et al. 2012) in Xinglong Observatory, the Multi-channel Photometric Survey Telescope (Mephisto, Yuan et al. 2020) and the Gamma-Ray Burst Optical/Near-Infrared Detector (GROND, Greiner et al. 2008) at the MPG 2.2 m telescope at ESO’s La Silla Observatory. The observational log is listed in Table B.2 and the data reduction of these observations is detailed in Section A.3.

2.3. Radio

Follow-up observations of EP J182730.0-095633 were conducted in the radio band with two ground telescopes, *ATCA* and *MeerKAT* (Camilo et al. 2018; Jonas 2018). Two *ATCA* observations were carried out on September 12th (Wang et al. 2024a) and September 21st, 2024. *MeerKAT* observed the source for three times, on September 21st, October 21st and October 28th, 2024. The observational log is listed in Table B.3 and the data reduction of these observations is detailed in Section A.4.

3. DATA ANALYSIS AND RESULTS

3.1. X-ray spectral analysis

The X-ray spectral analysis was performed using *XSPEC* v12.14.0b (Arnaud 1996), based on data collected post-September 4th from *EP/WXT*, *EP/FXT*, *NICER*, *Swift*, and

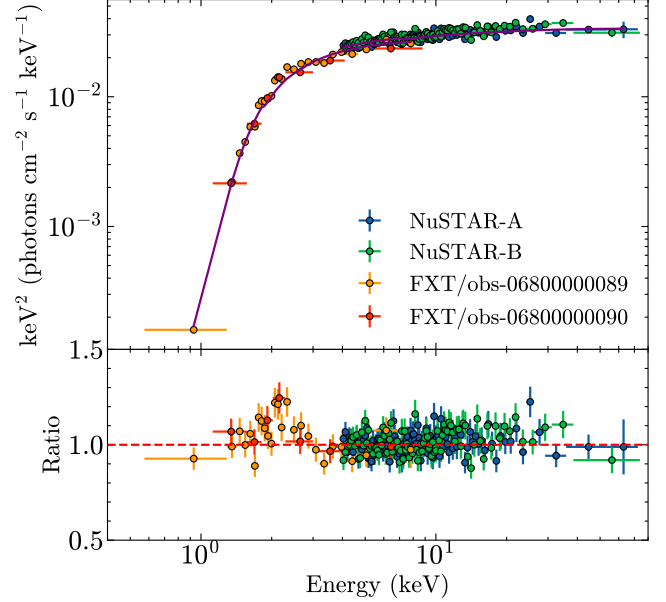


Figure 2. Joint spectral fitting of *EP/FXT* (module B, 0.5–10 keV) and *NuSTAR* (4–79 keV) with an absorbed cutoff power-law model. Note that the residual feature at ~ 2 keV is due to a calibration issue.

NuSTAR. The energy bands used for spectral fitting were 0.5–4 keV (*EP/WXT*), 0.5–10 keV (*EP/FXT*), 0.5–10 keV

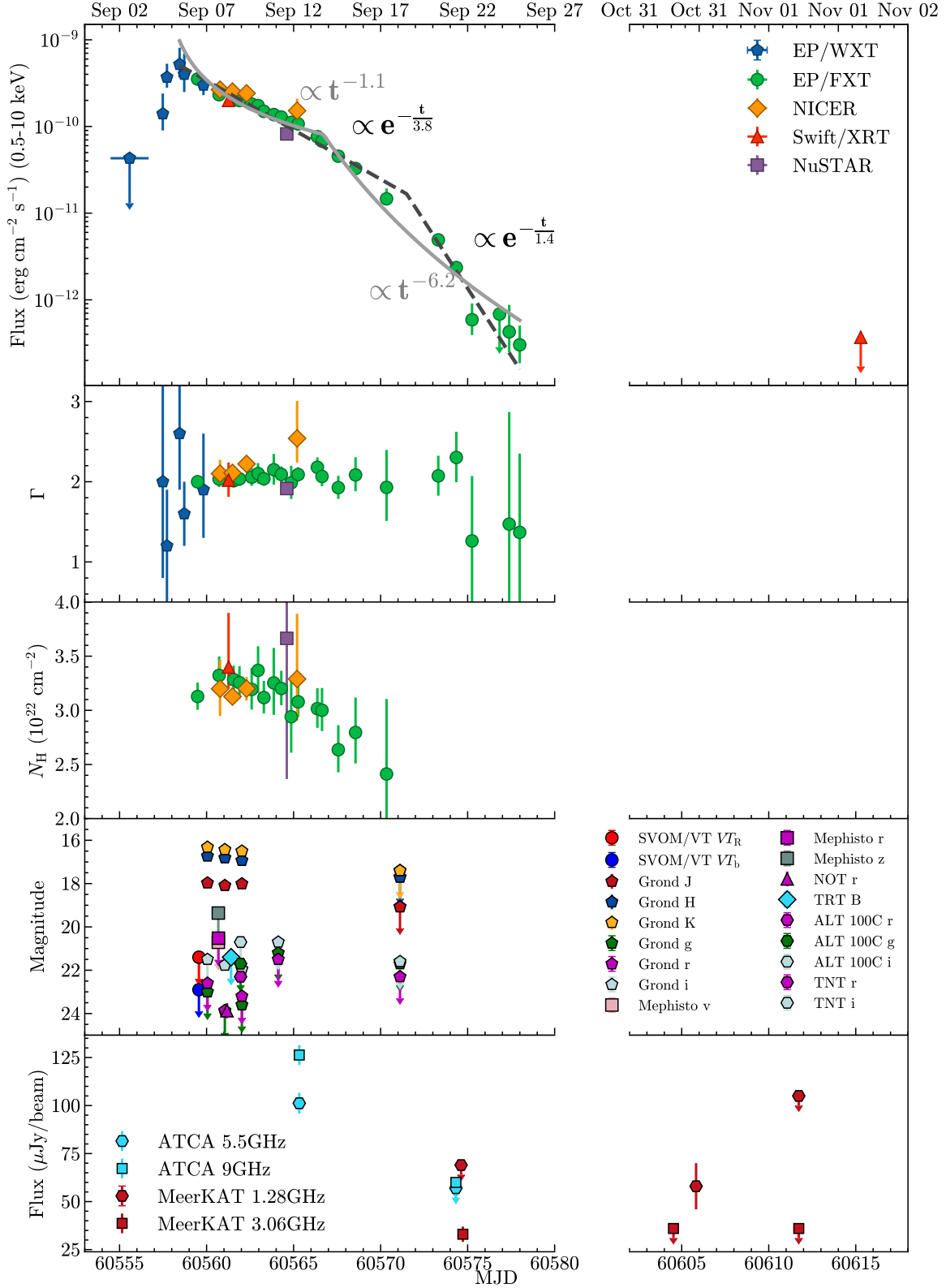


Figure 3. Long-term evolution of the multi-wavelength properties of EP J182730.0-095633. Top to bottom panels: the evolutions of the unabsorbed flux in the 0.5–10 keV band, the photon index (Γ), the hydrogen column density (N_H), the observed magnitude in the optical/infrared bands, and the radio peak flux density of *ATCA* and *MeerKAT*, respectively. The X-ray flux during the decaying phase is fitted either by a broken power-law model (the gray solid curve), or a broken exponential model (the black dashed curve). See Section 3.2.1 for more details. The results of a few optical/infrared observations after the X-ray outburst, where only upper limits have been obtained, are not shown for clearer data visualization. Also, primarily due to the low S/N of the data, the X-ray absorbing column density N_H in some observations cannot be well constrained within physically reasonable ranges and are fixed at $3.1 \times 10^{22} \text{ cm}^{-2}$, hence they are not shown in this figure (see text and Table B.1 for more details).

(*NICER*), 0.3–10 keV (*Swift*), and 4–79 keV (*NuSTAR*). The *Swift*, *NICER*, *NuSTAR*, and *EP/FXT* spectra before September 20th were grouped with a minimum of 25 counts per bin, and the best fit was determined by minimizing the χ^2 statistic. The *EP/FXT* spectra after September 20th as well as the *EP/WXT* spectra, due to the lower number of counts, were grouped with a minimum of 2 counts per bin, and the best fit was obtained by minimizing the Cash statistic (Cash 1979). All uncertainties are reported at the 90% confidence level for a single parameter of interest unless otherwise stated.

We began the spectral fitting using a simple absorbed power-law model (`tbabs*powerlaw` in XSPEC). The abundances were set to WILM (Wilms et al. 2000) and the cross-sections were set to VERN (Verner et al. 1996). In most cases, all parameters including the column density N_{H} , the photon index Γ , and the normalization are allowed to vary. However, due to the low spectral quality of the WXT observations from September 4th to 6th and the FXT observations after September 20th, N_{H} could not be constrained within physically meaningful ranges. Therefore, we fixed N_{H} at $3.1 \times 10^{22} \text{ cm}^{-2}$, derived from the FXT observation on September 6th, which offered the best spectral quality. A simple absorbed power-law model yields acceptable fits for all spectra. The fitted parameters are summarized in Table B.1. We also tested the spectral fitting with the blackbody (`tbabs*bbbodyrad`) or disk blackbody (`tbabs*diskbb`) model. However, neither of them provides a satisfactory fit. In addition, we performed a joint spectral fitting using the simultaneous *EP/FXT* and *NuSTAR* observations taken on September 11th. A Constant model was applied to correct for calibration differences between different telescopes, with *NuSTAR*/FPMA fixed at unity as the reference. Across the wide energy range of 0.5–79 keV, the spectra are still represented by the absorbed power-law model, with no evidence of iron line signatures and thermal contributions, resulting in a fit statistic of $\chi^2/\text{d.o.f} = 1002.40/1011$ and a photon index of 1.91 ± 0.01 . On this basis, although the `powerlaw` model has already provided a statistically acceptable fit, we further tentatively test the fits and estimate the high-energy cutoff by replacing the `powerlaw` model with two models, `cutoffpl` (refer to Figure 2 for an example) and `nthcomp` (Zdziarski et al. 1996; Życki et al. 1999), respectively. Both models provide an equivalently-acceptable fit compared with that of the `powerlaw` model. For the former, the cutoff energy is larger than 200 keV. The `nthcomp` model, on the other hand, yields a stringent constraint of $T_{\text{e}} > 30 \text{ keV}$, with the blackbody temperature parameter inherent in this model fixed at a typical value of 0.1 keV. In both cases, the best-fitting column density and photon index are consistent with those obtained using the simple absorbed power-law model. In short, we

conclude that the X-ray spectrum of EP J182730.0-095633 is dominated by non-thermal emission.

The unabsorbed source flux in the 0.5–10 keV band is calculated using the `cflux` model in XSPEC. To determine the upper limit of the pre-outburst X-ray brightness, we stack the WXT data from September 1st to 3rd, utilizing the same source extraction and background regions as for the real detection observations. The count rate is then converted to flux using the factor derived from the first WXT detection, under the assumption that the spectral shape remained stable during the rising phase of the outburst. It is worth noting that, while this assumption may not be entirely physically justified, the main conclusions should remain unaffected. At the end of the outburst, the source was not detected in the second *Swift*/XRT observation. We determine the upper limit of the count rate from the 0.5–10 keV image, and then evaluate the post-outburst flux using WEBPIMMS tool³ with assumptions of $N_{\text{H}} = 3.1 \times 10^{22} \text{ cm}^{-2}$ and $\Gamma = 2.0$, representing the typical spectral parameters during the outburst.

3.2. X-ray temporal analysis

3.2.1. Long-term X-ray behavior

In Figure 3, we present the long-term evolutionary trend of X-ray flux, Γ , and N_{H} during the outburst. The full outburst lasted approximately three weeks, during which the source’s flux varied by more than three orders of magnitude. Following a rapid rise to a peak flux of approximately $5.2 \times 10^{-10} \text{ erg s}^{-1} \text{ cm}^{-2}$ on September 5th, the flux gradually decreased to a minimum of $\sim 2 \times 10^{-13} \text{ erg s}^{-1} \text{ cm}^{-2}$ on September 24th. The decline phase displays a two-stage pattern. When employing a broken power-law model to fit the long-term light curve, there is an initial slow decay of $t^{-1.1}$ transitioning to a more rapid drop of $t^{-6.2}$, occurring 9.3 days after the source’s discovery. Alternatively, when using a broken exponential decay model, which provides a better fit, a transition is observed at 14.1 days. Prior to this transition, the flux decreases at a rate of $e^{-\frac{t/1 \text{ day}}{3.8}}$, which accelerates to $e^{-\frac{t/1 \text{ day}}{1.4}}$ after the break. This dual decay pattern might correspond to different underlying physical mechanisms.

Although there are evident changes in the source’s brightness, Γ remains fairly stable, exhibiting a consistent value of ~ 2 throughout the outburst. On the other hand, the column density N_{H} slightly decreases from $\sim 3 \times 10^{22} \text{ cm}^{-2}$ to $\sim 2 \times 10^{22} \text{ cm}^{-2}$ between September 6th and September 17th, suggesting that the origin of X-ray absorption is intrinsic to the source. The observed excess above the Galactic HI column density in the direction of the source, which is around $1.13 \times 10^{22} \text{ cm}^{-2}$ as determined using the HI4PI Survey map (HI4PI Collaboration et al. 2016) accessed through

³ <https://heasarc.gsfc.nasa.gov/cgi-bin/Tools/w3pimms/w3pimms.pl>

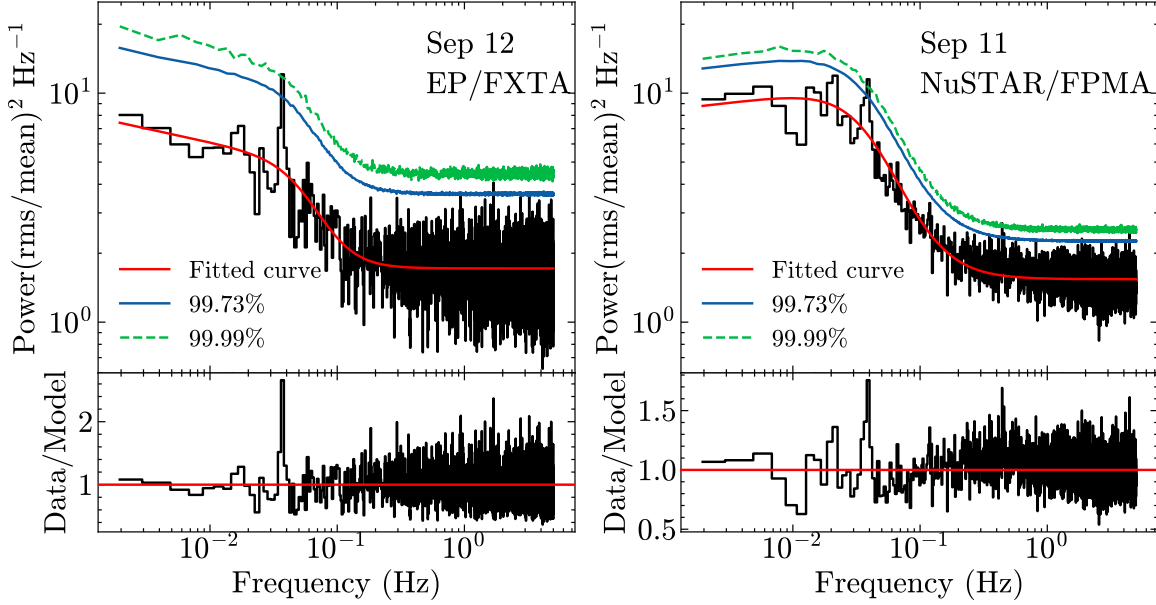


Figure 4. Power density spectra of the *EP/FXTA* (left panel, ObsID 06800000091) and *NuSTAR* data (right panel, ObsID 91001334002), with the bottom of each panel showing the power ratio between the data and best-fitting bending power-law model.

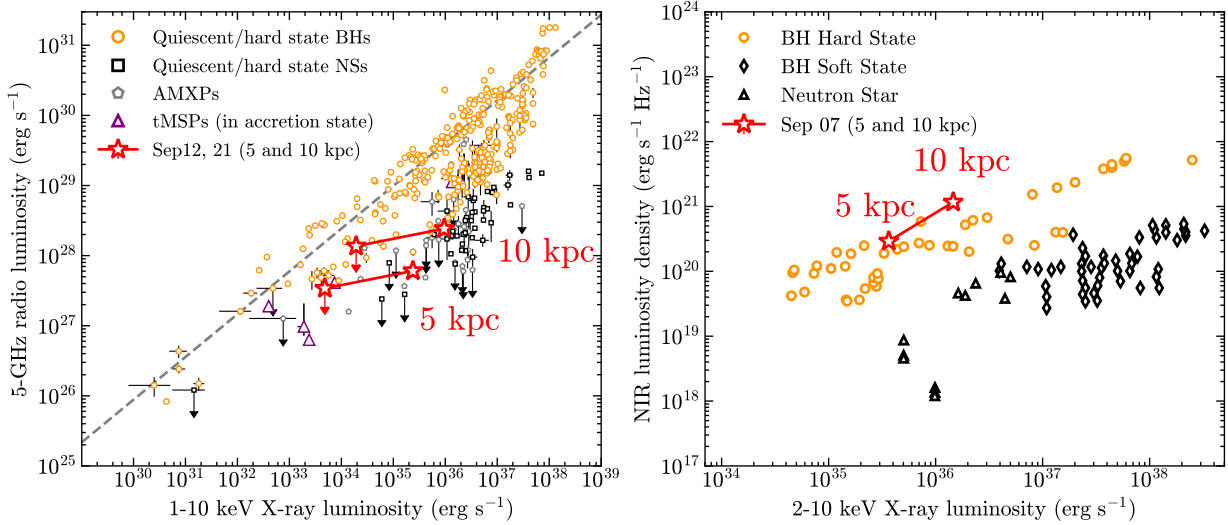


Figure 5. Quasi-simultaneous X-ray versus radio and near-infrared luminosities for LMXBs including EP J182730.0-095633. Left: the radio–X-ray (L_R – L_X) fundamental plane for X-ray binaries, adopted from [Bahramian & Rushton \(2022\)](#). The results of EP J182730.0-095633 are represented by red symbols, assuming various distance values. Right: the position of EP J182730.0-095633 on the near-infrared–X-ray ($L_{\text{NIR(JHK)}}$ – L_X) correlation for X-ray binaries ([Russell et al. 2006](#)). The data are taken on September 7th (the results barely change for those of September 8th and September 9th), and corrected for absorption using extinction values of $A_H = 2.8 \pm 0.1$ mag. For brevity, only the results of the *H* band are displayed here as a representative, with similar results for the other two bands.

the HEASARC online tool ⁴, also supports this interpretation. We also calculated the evolutionary trend of the spectral index while keeping the column density fixed at the typical value of $3.1 \times 10^{22} \text{ cm}^{-2}$, yielding results consistent with

those presented above within measurement uncertainties (see Figure B.1 for an illustration).

3.2.2. Short time-scale variability

We conducted a search for thermonuclear X-ray bursts and pulsations in all available X-ray data, as these phenomena serve as strong evidence for identifying the source in a neutron star (NS) system. However, no thermonuclear X-ray bursts were identified in the light curves. Additionally,

⁴ <https://heasarc.gsfc.nasa.gov/cgi-bin/Tools/w3nh/w3nh.pl>

no significant pulsations were detected in the power spectra, with 3σ upper limits on the flux pulsed fraction of 6%–10% for the second *NICER* observation, 8%–13% for the *NuSTAR* observation, and 6%–13% for the *EP/FXT* observations across the frequency range 30–1000 Hz (for more details, see Appendix A.2). Although the light curves do not show thermonuclear X-ray bursts or pulsations, they present strong short-time variations. We conducted a power spectral density (PSD) analysis using a timing resolution of 0.1 s, and a segment length of 256 s or 512 s. For most observations a segment length of 512 s is adopted, while for observations with relatively short GTIs, a 256 s segment length is chosen for a higher signal-to-noise ratio in resulting PSD. The PSD is normalized in units of rms^2 per Hz (Belloni & Hasinger 1990). Figure 4 displays the PSDs for the observations taken by *EP/FXTA* and *NuSTAR/FPMA*. The continuum component of both PSDs exhibits increased noise towards lower frequencies (red noise) and can be well modeled by a bending power-law function with a break frequency of around 0.03–0.06 Hz. Additionally, there is a prominent, narrow peak around 0.038 Hz, indicating the presence of a quasi-periodic oscillation (QPO) with an RMS amplitude of $\sim 20\%$. To assess the significance of the QPO, we simulated one hundred thousand light curves, based on the method of Timmer & König (1995) from the best-fit bending power-law PSD. We then calculated the PSDs of these light curves, and determined the distribution of the variability power at each Fourier frequency. The significance of the QPO greatly exceeds the 3σ confidence threshold, with the quality factor $q \equiv \nu_0/(2\Delta\nu)$ estimated to be $\gtrsim 8$. The QPO is also present in the FXT module B (FXTB) data, collected in the Partial Window (PW) mode, with a centroid frequency, significance, and q -factor that roughly match those found in the FXTA data. The QPO feature is evident in other FXT observations before September 20th, as shown in Figure B.2, with the centroid frequency remaining around 0.04 Hz despite the X-ray flux varying by more than two orders of magnitude. After September 20th, no clear QPO signal was observed, probably because of the very low count rate of the source. In addition, a similar QPO is also detected in the *NICER* data, although with lower significance of about 2σ (Figure B.2).

3.3. Optical and infrared detection

SVOM/VT rapidly responded to observe the field of EP J182730.0-095633 on September 6th, yet no uncatalogued objects were detected within the *Swift*/XRT error circle. The 5σ upper limits for the VT_R (650 - 1000 nm) and VT_B (400 - 650 nm) bands are 21.4 mag and 22.9 mag, respectively. From September 7th to 9th, this field was extensively observed by several instruments, including GROND, NOT, Mephisto, TRT and ALT100C. The observations of Mephisto, TRT and ALT100C did not uncover any new or

flaring objects around the X-ray position, but an uncatalogued source was detected by GROND in the near-infrared (NIR) J , H and K_s bands in all three epochs (see panels (e) and (f) in Figure 1), with consistent magnitudes of $J \sim 18$ mag, $H \sim 16.8$ mag and $K_s \sim 16.4$ mag, all in the AB system (see Table B.2). The position of the NIR signal is R.A. = $18^{\text{h}}27^{\text{m}}30.09^{\text{s}} \pm 0.01^{\text{s}}$ and Decl. = $-9^{\circ}56'39.6'' \pm 0.2''$. It is worth noting that the signal was also marginally detected by NOT in the r band on September 7th (with a magnitude of 23.87 ± 0.35 mag; Fu et al. 2024), as well as by GROND in both r' and i' bands on September 8th (with magnitudes of 23.86 ± 0.30 mag and 21.77 ± 0.10 mag, respectively). Interestingly, this source was no longer detected in the following GROND observations carried out on September 11th and thereafter, clearly indicating a fading behavior. Additionally, at the end of the X-ray outburst, *SVOM/VT* and TNT carried out two additional observations for this field on September 28th and October 11th, respectively, yet no sources were detected. The long-term evolution of the apparent magnitudes during the X-ray outburst is shown in the bottom panel of Figure 3.

The faint optical and near-infrared detection is likely due to high extinction, given the low Galactic latitude of EP J182730.0-095633. Specifically, in the source direction the Galactic foreground reddening in the V band is very severe, with $A_V \sim 15.4 - 15.8$ mag (Schlafly & Finkbeiner 2011) accessed through dust extinction tools on NED⁵ and IRAS⁶. The reddening for the GROND J and H band are estimated to be 4.4 ± 0.1 mag and 2.8 ± 0.1 mag, respectively, by applying the relationship between A_λ and A_V taken from Cardelli et al. (1989). We take these values for subsequent NIR luminosity calculations (see Section 4). The results of GROND and *EP/FXT* observations during when the source was detected by GROND from September 7th to 9th were taken for the investigation of the L_X - L_R correlation, as shown in the right panel of Figure 5.

3.4. Radio detection

The first *ATCA* observation on September 12th identified a radio source at the X-ray position (Figure 1). At 5.5 GHz, the source position was R.A. = $18^{\text{h}}27^{\text{m}}30.16^{\text{s}} \pm 0.39^{\text{s}}$ and Decl. = $-9^{\circ}56'36.0'' \pm 3.51''$, while at 9 GHz, it was located at R.A. = $18^{\text{h}}27^{\text{m}}30.07^{\text{s}} \pm 0.21^{\text{s}}$ and Decl. = $-9^{\circ}56'40.4'' \pm 2.09''$. The radio locations are $5.4 \pm 4.1''$ and $1.0 \pm 3.0''$ away from the *Swift* X-ray position respectively. The peak flux densities at 5.5 GHz and 9 GHz were measured to be $101.2 \pm 5.4 \mu\text{Jy/beam}$ and $126.3 \pm 5.2 \mu\text{Jy/beam}$, respectively. The radio spectral index (α) is 0.45 ± 0.14 , showing an inverted spectrum. During a subsequent *ATCA* observation,

⁵ https://ned.ipac.caltech.edu/extinction_calculator

⁶ <https://irsa.ipac.caltech.edu/applications/DUST/>

conducted on September 21st, no significant radio emission was detected, yielding 3σ upper limits of $57 \mu\text{Jy/beam}$ at 5.5 GHz and $60 \mu\text{Jy/beam}$ at 9 GHz. A slight positional offset ($\sim 4.5''$) was observed between the centroids at the two frequencies in the first *ATCA* observation, with a significance level of 3σ . It remains unclear whether this discrepancy is due to intrinsic physical processes or systematic errors from instrumental effects, as the source was undetectable in later observations. The results of *EP/FXT* and *ATCA* observations on September 12th and 21st were taken for the investigation of the L_X - L_R correlation, as shown in the left panel of Figure 5.

In the first *MeerKAT* epoch we obtained a detection at S-band (3.06 GHz) in which the source located at R.A. = $18^{\text{h}}27^{\text{m}}30.00^{\text{s}} \pm 0.009^{\text{s}}$ and Decl. = $-9^{\circ}56'39.75'' \pm 0.13''$, with a flux density of $33 \pm 4 \mu\text{Jy}$. While at L-band (1.28 GHz) we have a non-detection, with a 3σ upper limit of $69 \mu\text{Jy/beam}$. The source position obtained by *MeerKAT* is consistent with those provided by *Swift*/XRT and *ATCA* at 9 GHz. The spectral shape of *MeerKAT* is also consistent with the positive spectral index obtained in the first *ATCA* epoch. In our second *MeerKAT* epoch we obtain a detection at L-band at $58 \pm 12 \mu\text{Jy}$, and a non-detection at S-band with a $36 \mu\text{Jy/beam}$ 3σ upper limit. Finally, we obtained no-detections at both L- and S-band in our third *MeerKAT* epoch, with $105 \mu\text{Jy/beam}$ and $36 \mu\text{Jy/beam}$ upper limits, respectively. The results of *ATCA* and *MeerKAT* are summarized in Table B.3.

4. DISCUSSION

4.1. Nature of the transient

EP J182730.0-095633 (EP240904a) is a new X-ray transient discovered by *EP/WXT* on September 4th, 2024. Follow-up observations were performed with multiple X-ray telescopes and multi-wavelength facilities. In this paper, we report on the spectral and temporal properties of this source derived from the outburst, aiming to uncover its physical nature.

At the corresponding location of EP J182730.0-095633, a faint NIR transient source was detected by GROND and NOT. The NIR flux showed a rapid decay and became undetectable within a few days, accompanied by a simultaneous decline in the X-ray flux. Given its spatial and temporal coincidence, we suggest that the transient source detected by GROND and NOT is very likely to be associated with EP J182730.0-095633, thus representing a promising candidate for the NIR counterpart. We note that the non-detection of the signal in optical bands can be attributed to the large Galactic foreground reddening of $A_V \approx 15.4 - 15.8$ mag along the line-of-sight.

Due to the faintness and rapid diminishing of the potential counterpart, no optical/NIR spectrum was obtained, and thus no redshift measurement could be made. The absence

of a redshift measurement complicates the task of determining the source's nature. However, it is largely unlikely that this transient is either a Gamma-Ray Burst (GRB) or a stellar flare due to the differing characteristics. GRBs generally exhibit a much shorter timescale for their rise and decay, with the former typically occurring within a few seconds and the latter lasting a few days (Zhang et al. 2006), whereas stellar flares are characterized by X-ray spectra primarily described by one or several optically thin thermal plasma components (Benz & Güdel 2010).

The tidal disruption event (TDE) may be a potential scenario, given that some of the observational properties of EP J182730.0-095633, such as the non-thermal X-ray spectrum, two-stage decaying trend as well as the radio and infrared detections, are broadly consistent with a rare class of TDEs dominated by relativistic jet (e.g. Burrows et al. 2011; Bloom et al. 2011; Pasham et al. 2015). However, the infrared-to-X-ray flux ratio appears to be significantly higher compared to that observed in jetted TDEs (e.g. Pasham et al. 2015; Levan et al. 2016). Meanwhile, we do not observe a plateau phase or strong intra-day variability in X-rays which instead are common features in those jet-dominated systems. Therefore, the possibility of EP J182730.0-095633 being a jetted-TDE seems less unlikely. Moreover, it is interesting to point out that, despite numerous differences, EP J182730.0-095633 has exhibited a PSD profile similar to a rare white dwarf (WD) - terrestrial-icy planet TDE candidate IGR J17361-4441 (Bozzo et al. 2011; Del Santo et al. 2014) discovered by the IBIS/ISGRI telescope (Ubertini et al. 2003) onboard *INTEGRAL* on 2011 August 11, which shows a notable QPO signal with a centroid frequency of ~ 100 mHz (Bozzo et al. 2014).

In contrast, EP J182730.0-095633 resembles XRBs in a variety of aspects regarding the source position, radio emission, X-ray variability, spectral properties, and multi-wavelength relationships. Firstly, the position of EP J182730.0-095633 is on the Galactic plane, a region densely populated by X-ray binaries (e.g. Grimm et al. 2002; Bahramian & Degenaar 2023). Secondly, the X-ray flux of EP J182730.0-095633 generally follows a fast-rise-exponential-decay behavior (FRED), which agrees largely with the canonical outburst behavior of XRBs (Chen et al. 1997; Remillard & McClintock 2006). The multifold pattern during the decaying phase can also be interpreted within the context of XRB outbursts (e.g. King & Ritter 1998; Dubus et al. 2001; Weng & Zhang 2015). Thirdly, as shown in Figure 5, EP J182730.0-095633's positions on the L_X - L_R and L_X - L_{NIR} diagrams are in good agreement with an XRB origin, assuming a distance of several kpc. Additionally, the radio detection, combined with an inverted radio spectrum obtained by *ATCA* and *MeerKAT*, may suggest the presence of a compact jet, which is commonly observed in the hard

states of XRBs (see Belloni 2010, and references therein). This possibility is further supported by the observed non-thermal power-law spectrum, a characteristic feature in the hard states. The spectral shape variation in the radio band during the late outburst stage implies that the compact jet transitioned from optically thick to optically thin state (see Section 3.4), a phenomenon commonly observed during the decay phase of XRB outbursts (e.g. Corbel et al. 2013; Díaz Trigo et al. 2018). More importantly, the QPO signal, which is a prevalent feature in XRBs (Ingram & Motta 2019), is significantly detected during a long period of the outburst.

4.2. Properties of the accreting system

If EP J182730.0-095633 is a Galactic XRB, the peak X-ray luminosity ($L_{2-10 \text{ keV}}$) is estimated to be $\lesssim 10^{36} \text{ erg s}^{-1}$, assuming a distance of several kpc. According to Wijnands et al. (2006), it can then be classified as a borderline faint to very faint XRB (VFXB). These sources were recently and extensively discovered in the Galactic Center, Galactic Plane, and Galactic Bulge by *ASCA*, *Swift*, *Chandra* and *XMM-Newton* surveys (e.g. Hands et al. 2004; Munro et al. 2005a,b; Sakano et al. 2005; Degenaar & Wijnands 2009, for a detailed review, one may refer to Bahramian & Degenaar (2023)). Their outbursts typically last for several weeks to months (e.g. Degenaar & Wijnands 2009; Heinke et al. 2015; Weng & Zhang 2015).

Identifying the nature of the central compact object (NS or BH) is somehow challenging for EP J182730.0-095633, due primarily to the lack of definitive evidence supporting either scenario (e.g. coherent pulsations, thermonuclear bursts or dynamical mass estimation). Its locations on the radio vs. X-ray luminosity fundamental plane (see left panel of Figure 5) fall onto the overlapping regions of BHs and NSs, yielding inconclusive argument. Nevertheless, we are inclined to argue that EP J182730.0-095633 is more likely to be a BH XRB for the following reasons. Firstly, the X-ray emission throughout the outburst is consistently described by a non-thermal power-law spectrum with a photon index maintaining at ~ 2 . This ‘stable’ behavior largely precludes the source being a NS accreting system as the spectrum of the latter often exhibits a softening trend as the luminosity decreases below $10^{36} \text{ erg s}^{-1}$ due to the presence and growing prominence of the NS surface emission (Wijnands et al. 2015). This dichotomy in the spectral shape evolution has been increasingly studied in recent years (e.g. Plotkin et al. 2013; Wijnands et al. 2015; Qiao & Liu 2020), and developed to be a diagnostic tool for identifying BH (candidates) (e.g. Stoop et al. 2021). Secondly, the relative strength of the X-ray and NIR emissions (Figure 5) closely aligns with those typically observed in BH binaries in the hard state (Russell et al. 2006). Thirdly, the joint spectral fitting of EP/FXT+*NuSTAR* data indicates a relatively high electron

temperature of $T_e > 30 \text{ keV}$ (see Section 3.1), which is more prone to exist in BH systems (e.g. Burke et al. 2017; Banerjee et al. 2020). Furthermore, even though mHz QPOs are detected in a number of NS systems and are usually attributed to the marginally stable nuclear burning on the NS surface (e.g. Revnivtsev et al. 2001; Strohmayer & Smith 2011; Mancuso et al. 2019; Lyu et al. 2020; Mancuso et al. 2023; Tse et al. 2023), the only two VFXBs with QPO detection, Swift J1357.2-933 (Armas Padilla et al. 2014; Beri et al. 2023) and XTE J1118+480 (Revnivtsev et al. 2000; Wood et al. 2000), have been confirmed to host BH accretors. Future observations, particularly dynamical mass measurements, are essential to verify this scenario and unveil the mysterious nature of EP J182730.0-095633.

Regarding the companion star, its nature remains largely inconclusive due to the current lack of spectroscopic information. However, we can tentatively explore this issue based on the quasi-quiescent NIR luminosity, assuming that it is contributed mainly by the companion. Specifically, considering the upper limit of $m_J > 19.2 \text{ mag}$ given by GROND observations on September 18th (near the end of the X-ray outburst), the corresponding absolute magnitude upper limit is $M_J > 4.7 \text{ mag}$ assuming a distance of 10 kpc and a Galactic foreground dust extinction of $A_J = 4.4 \text{ mag}$. According to typical stellar parameters (Pecaut et al. 2012; Pecaut & Mamajek 2013), the companion star is likely a late type K/M star, indicating that this source is a potential low-mass XRB.

The X-ray outburst of EP J182730.0-095633 resembles the ‘hard-only’ outbursts widely observed in X-ray binaries (e.g. Yan & Yu 2015; Tetarenko et al. 2016; Alabarta et al. 2021), which are notably characterized by the absence of state transitions. Its X-ray spectra show no iron $K\alpha$ line or thermal component, indicating that the standard Shakura-Sunyaev disk (SSD, Shakura & Sunyaev 1973) is either absent or truncated at a large radius. The accretion close to the compact object is likely to operate in the form of an optically thin, geometrically thick advection-dominated accretion flow (ADAF, Ichimaru 1977; Narayan & Yi 1994, 1995a,b; Yuan & Narayan 2014). The observed X-ray spectral index remains relatively constant throughout the entire outburst, suggesting that the geometry of the accretion flow is relatively stable during the flaring activity. In such a scenario, the mHz QPOs, potentially generated by Lense-Thirring precession or quasi-periodic obscurations (as discussed in Beri et al. 2023), could exhibit stable frequencies, as observed.

We also note that there is another possibility that EP J182730.0-095633 is an extragalactic XRB system. If the correlation between X-ray and radio emissions is expected to follow the L_X - L_R relation typical of XRBs, its estimated distance would be within $\sim 10^2 \text{ kpc}$. However, there are no nearby satellite galaxies in the direction of EP J182730.0-

095633 (Drlica-Wagner et al. 2020), making this scenario less likely.

4.3. mHz QPO signal

Despite of the ubiquitous nature of QPOs in BHXRBs across various spectral states, the detection of the mHz QPO remains relatively rare (Ingram & Motta 2019), with only a few cases reported in the past few years, e.g. MAXI J1820+070 (Li et al. 2025), H 1743–322 (Altamirano & Strohmayer 2012) and MAXI J1348–630 (Wang et al. 2024b). The centroid frequency of the mHz QPO, falls within the range of type-C low-frequency QPOs (LFQPO), the most common type of QPO in X-ray binaries (e.g. Motta et al. 2011; Buisson et al. 2019). To tentatively probe the association of this ~ 40 mHz QPO signal with the commonly-observed type-C QPOs, we calculate the fractional-rms spectrum of QPO using the data of *EP-FXT* and *NuSTAR* obtained on September 11th 2024, as shown in the left panel of Figure B.3. Regardless of a large uncertainty, the rms-energy spectrum exhibits an enhanced fractional variability with the increasing photon energy below ~ 20 keV, then tends to flatten toward higher energies. This is generally consistent with that observed in type-C LFQPOs of XRBs (e.g. Casella et al. 2004; Rodriguez et al. 2004; Yadav et al. 2016; Yang et al. 2024). We further calculate the relation between the QPO frequency and the low-frequency PSD break for QPO detections with significance exceeding 3σ , as presented in the right panel of Figure B.3. The measurement of the EP transient is denoted in blue circles and the canonical W-K relation built for type-C LFQPOs (Wijnands & van der Klis 1999) is signified in black dashed line. Notably, the mHz QPO of EP J182730.0-095633 exhibits a much lower centroid frequency than predicted by the empirical W-K relation, also the QPO frequency remains quite stable despite of the variations in the PSD break. This makes it much less likely to be a typical type-C QPO. In this context, the QPO detected in EP J182730.0-095633 may represent a new class of LFQPOs in BHXRBs. It is also interesting to point out that the relative position of break and QPO looks similar to the low-frequency QPOs found in some Ultra-Luminous X-ray sources (ULXs, e.g. Dewangan et al. 2006; Atapin et al. 2019; El Byad et al. 2025). We note that a detailed investigation on the origin of this ~ 40 mHz QPO is beyond the scope of this paper and will be deferred to future work.

5. CONCLUSIONS

In this *Letter*, we report on the discovery and multi-wavelength follow-up observations of an intriguing X-ray transient EP J182730.0-095633 (EP240904a). This transient was first detected by *EP/WXT* on September 4th, 2024, with its location on the Galactic plane ($l = 21.3634^\circ$, $b =$

0.7244°). The source underwent a faint ($F_{\text{peak}, 0.5-10 \text{ keV}} \approx 5.2 \times 10^{-10} \text{ erg s}^{-1} \text{ cm}^{-2}$), short-lived (~ 20 days) outburst. The X-ray emission is of non-thermal origin, with the spectrum well described by a power-law model with a photon index (Γ) maintaining at ~ 2 . A relatively high electron temperature ($T_e > 30 \text{ keV}$) is inferred from the joint fit of *EP/FXT*+*NuSTAR* spectra using the *nthcomp* model. No thermonuclear bursts or significant coherent pulsations are detected in X-ray data, while a long-lasting millihertz QPO signal with a centroid frequency of $\sim 0.04 \text{ Hz}$ is significantly detected by various X-ray instruments. A radio source displaying an inverted spectrum ($\alpha = 0.45 \pm 0.14$), as well as a potential, transient NIR counterpart, are detected at the X-ray position.

Based on the source position, X-ray spectral and timing properties (stable evolution of Γ , high electron temperature, and the detection of mHz QPO), the radio spectral shape, as well as the multi-wavelength properties (the L_X - L_R and L_X - L_{NIR} correlations and the quasi-quietescent NIR brightness), we conclude that EP J182730.0-095633 is very likely to be a new black hole low-mass X-ray binary captured during a faint outburst without state transitions. The discovery of EP J182730.0-095633 showcases *EP*'s potential to find transient BHs exhibiting faint X-ray outbursts, which represent a potentially large population yet are mostly elusive to the other X-ray wide-field monitoring instruments. More of such systems are expected to be discovered in the *EP* era, which may advance our understandings of the underlying physical mechanism of faint-level outbursts, and hopefully shed light on the “missing” puzzle of black holes in our galaxy.

Facilities: *Einstein Probe* (Yuan et al. 2022), *Swift* (Gehrels et al. 2004), *NICER* (Gendreau et al. 2016), *NuSTAR* (Harrison et al. 2013), *Insight-HXMT* (Zhang et al. 2020), *SVOM* (Wei et al. 2016), *GROND* (Greiner et al. 2008), *Mephisto* (Yuan et al. 2020), *TNT* (Huang et al. 2012), *ATCA*, *MeerKAT* (Camilo et al. 2018; Jonas 2018).

Software: WXTDAS v1.0, fxtDas v1.10, HEASOFT v6.33.2 (Nasa High Energy Astrophysics Science Archive Research Center (Heasarc) 2014), Matplotlib v3.9 (Hunter 2007), NICERDAS v12, NuSTARDAS v2.1.4, XSPEC v12.14.0h (Arnaud 1996), PRESTO (Ransom et al. 2002), Source Extractor v2.28.0 (Bertin & Arnouts 1996), IRAF v2.16 (Tody 1986), CASA (CASA Team et al. 2022).

ACKNOWLEDGMENTS

We thank the anonymous referee for comments that help improve the paper. This work is based on data obtained with *Einstein Probe*, a space mission supported by Strategic Priority Program on Space Science of Chinese Academy of Sciences, in collaboration with ESA, MPE and CNES. This work is supported by the National Natural Science Founda-

tion of China (Grant Nos. 12203071, 12333004, 12122306, 12173048, 12473047, 12473016, 12373049, 12433007, 12361131579), the National Key Research and Development Program of China (Grant Nos. 2023YFA1607903, 2024YFA1611603, 2024YFA1611604), the National SKA Program of China (2022SKA0130100), the Tianshan Talent Training Program (2023TSYCCX0101), and the Strategic Priority Research Program of the Chinese Academy of Sciences (Grant No. XDB0550200). FCZ, AM and NR are supported by the European Research Council (ERC) via the consolidator grant “MAGNESIA” (No. 817661; PI: Rea), the proof of concept grant “DeepSpacePULSE” (No. 101189496; PI: Rea), the Spanish grant PID2023-153099NA-I00 (PI: Coti Zelati), the Catalan grant SGR2021-01269 (PI: Graber/Rea), and the program Unidad de Excelencia María de Maeztu CEX2020-001058-M. FCZ also acknowledges support from a Ramon y Cajal fellowship (grant agreement RYC2021-030888-I). RS acknowledges support from the INAF grant number 1.05.23.04.04. JPUF is supported by the Independent Research Fund Denmark (DFR-4090-00079) and thanks the Carlsberg Foundation for support. The Cosmic Dawn Center (DAWN) is funded by the Danish National Research Foundation under grant DNRF140. AB acknowledges support from the UK Space Agency. P.G.J. is supported by the European Union (ERC, Starstruck, 101095973). Views and opinions expressed are however those of the author(s) only and do not necessarily reflect those of the European Union or the European Research Council Executive Agency. Neither the European Union nor the granting authority can be held responsible for them.

This work is also based on data obtained by: the Neil Gehrels *Swift* Observatory (a NASA/UK/ASI mission) supplied by the UK *Swift* Science Data Centre at the University

of Leicester; *NICER*, a 0.2–12 keV X-ray telescope operating on the International Space Station, funded by NASA; the *NuSTAR* mission, a project led by the California Institute of Technology, managed by the Jet Propulsion Laboratory, and funded by NASA. We thank the *NICER* PI, Keith Gendreau, for approving our Target of Opportunity (ToO) request and the operation team for executing the observations; we thank the *Swift* deputy project scientist, Brad Cenko, and the *Swift* duty scientists and science planners, for making the *Swift* ToO observations possible; we also thank the *NuSTAR* PI, Fiona Harrison, for approving our Director’s Discretionary Time request, and the *NuSTAR* science operation center for carrying out the observation. The Australia Telescope Compact Array is part of the Australia Telescope National Facility (grid.421683.a) which is funded by the Australian Government for operation as a National Facility managed by CSIRO. We acknowledge the Gomeri people as the traditional owners of the Observatory site. The MeerKAT telescope is operated by the South African Radio Astronomy Observatory, which is a facility of the National Research Foundation, an agency of the Department of Science and Innovation. This work has made use of the “MPIfR S-band receiver system” designed, constructed and maintained by funding of the MPI für Radioastronomie and the Max-Planck-Society.

We acknowledge the data resources and technical support provided by the China National Astronomical Data Center, the Astronomical Science Data Center of the Chinese Academy of Sciences, and the Chinese Virtual Observatory. The storage and processing of the EP data are supported by Alibaba Cloud through its Creation Beyond Cloud Program. Part of the funding for GROND (both hardware as well as personnel) was generously granted from the Leibniz-Prize to Prof. G. Hasinger (DFG grant HA 1850/28-1)

APPENDIX

A. MULTI-WAVEBAND DATA REDUCTION

A.1. X-rays

A.1.1. Einstein Probe

EP J182730.0-095633 was first detected in an observation starting on September 4th, 2024, at 10:12:56 UT and lasting approximately 8.8 ks, on the CMOS detector No.39 of WXT (ObsID: 06800000067). Previous individual observations covering three days before the detection, as well as the stacked data, did not reveal any notable source signals. The WXT images from September 3rd to 4th (first detection) are shown in panels (a)–(b) of Figure 1. It is worth noting that for the observation on September 4th, the emission of the source is rather stable without short-term flaring activity. Following the discovery, an extensive monitoring campaign was conducted by EP/FXT from September 6th to 24th, with a cadence of twice per day during the first week and \sim once per day thereafter. A total of 22 FXT observations were conducted and utilized for analysis. We note that the source was too faint for detection on September 23rd (ObsID: 06800000118), due mainly to a significantly shorter exposure time of approximately \sim 1000 s. The FXT was operated with module A (FXTA) in Timing Mode (TM) and module B (FXTB) in Partial Window (PW) mode, except during the first observation, where both FXTA and FXTB were in Full Frame (FF) mode. The first

FXT observation provides a more precise localization of the source, with coordinates of R.A. (J2000.0) = $18^{\text{h}}27^{\text{m}}30.0^{\text{s}}$ and Decl. (J2000.0) = $-9^{\circ}56'33''$ (with an uncertainty of $10''$ at the 90% confidence level).

For *EP/WXT*, we take observations from September 1st to 6th for data analysis. Data reduction was performed using *wxtpipeline*, the standard pipeline of the WXT Data Analysis Software (WXTDAS, Liu et al. in preparation), and the calibration database (CALDB) developed by the EP Science Center (EPSC). The CALDB is built based on the results of the on-ground calibration experiments (Cheng et al. 2025), with the procedure successfully implemented on a prototype of the WXT instrument (Cheng et al. 2024a). *wxtpipeline* performs calibrations to the original event data, including the coordinate transformation, flagging bad and hot pixels, and computing the pulse height amplitude invariant (PI) values, then generates the clean event list by screening the events based on the default criteria ($\text{BR_EARTH} \geq 25$ & $\text{ELV} \geq 10$ & $\text{SAA} = 0$ & $\text{ANG_DIST} < 0.1$). The sky image and exposure map are extracted from the clean event list. A point-source detection is then implemented on the sky image. Sources of high significance (greater than 5σ , calculated using the Li-Ma method, Li & Ma 1983) are cataloged, creating a detection list. For each identified source, several outputs are produced, including the light curve and spectra, the ancillary response file, the response matrix, as well as the background light curve and spectra. The light curves and spectra are extracted using a circular region centered on the source, with a radius of $9.1'$. For the background, an annular region centered on the source is employed, with inner and outer radii of $18.2'$ and $36.4'$, respectively. The *wxtmerge* tool is utilized to stack multiple WXT observations.

Data reduction for FXT was performed using *fxtchain*, the standard data analysis pipeline within the FXT Data Analysis Software (FXTDAS, v1.10, Zhao et al. 2025) developed by EPSC. This tool includes several procedures, including: particle event identification, pulse-invariant value calculation, bad and hot pixel flagging, and the selection of good time intervals (GTIs) using housekeeping data. The source was bright in the first observation carried out in FF mode, leading to a non-negligible pile-up effect. To mitigate this effect the source photons were extracted using an annulus region centered on the target with an inner radius of $15''$ and outer radius of $80''$. The background photons were taken from a nearby source-free circular region with a radius of $150''$. For the PW imaging mode, the radius of the source and background circular regions were both set to $60''$. For the TM mode, the source and background photons were extracted using two rectangular regions centered on the source and away from the source, respectively, both with a size of $3' \times 1'$. The Solar System barycentric correction for photon arrival times was applied using the *fxtbary* tool. The TM data were excluded from the spectral analysis because of a lower spectral quality compared to those taken in the imaging mode.

A.1.2. *NICER*

Following the discovery of the source, *NICER* made several observations beginning on September 7th (PI: Huaqing Cheng). However, from September 23rd onwards (ObsID 7204340113), the source's flux fell below $10^{-12} \text{ erg s}^{-1} \text{ cm}^{-2}$, resulting in the *NICER/XTI* spectra with a considerable background noise. Consequently, these observations were excluded from the data analysis. For the observations before September 23rd, clean event files were produced using *nicerl2* with specific settings: `underonly_range="0-200"` and `overonly_range="0-2"`. Focal Plane Modules (FPMs) 14 and 34 were not included in the analysis as they often show elevated detector noise. Light curves and spectra were extracted using *nicerl3-lc* and *nicerl3-spec*, respectively, employing the SCORPEON background model⁷. This rigorous selection process resulted in only 4 observations (ObsIDs: 7204880101, 7204880102, 7204880103, and 7204880105) with clean events. Photon arrival times were corrected to the Solar System barycenter using the *barycorr* tool.

A.1.3. *Swift*

We conducted two target-of-opportunity (ToO) observations using the X-ray telescope (XRT) onboard the Neil Gehrels Swift Observatory (*Swift*) in the Photon Counting (PC) mode, one on September 8th, 2024 and another on November 1st, 2024 (PI: Huaqing Cheng). The source was significantly detected in the first *Swift* observation, while no signals were found in the second epoch. The XRT data were processed using *xrtpipeline*, and the spectra were extracted from the level-2 cleaned data products using *xselect*. The source photons were initially extracted from a circular region centered on the target with a radius of $47''$, while the background photons were extracted from a nearby source-free circular region with a radius of $188''$. However, the pile-up effect is found to be non-negligible as indicated by the high count rate of $\sim 1.5 \text{ counts s}^{-1}$. To mitigate the pile-up effects, photons within an inner radius of $8''$ were excluded. For the extracted X-ray spectra, we employed *xrtmkarf* to build the ancillary response files (ARF). The response matrix functions (RMFs) were then determined using the *quzcf* tool.

The first *Swift/XRT* observation provides a source position, which is enhanced by applying correction of the *Swift/UVOT* photometry (Evans et al. 2009): R.A. (J2000.0) = $18^{\text{h}}27^{\text{m}}30.1^{\text{s}}$ and Decl. (J2000.0) = $-9^{\circ}56'41.4''$ (uncertainty of $2.1''$ at the

⁷ https://heasarc.gsfc.nasa.gov/docs/nicer/analysis_threads/scorpeon-overview/

90% confidence level). The XRT position is consistent with the FXT position with a separation of $8''$ (note that the uncertainty of FXT position is $10''$). We adopt the XRT coordinates as the X-ray position of EP J182730.0-095633.

A.1.4. *NuSTAR*

NuSTAR carried out an observation on September 11th, 2024, with a total exposure time of approximately 20.7 ks (PI: Alessio Marino). The data were processed using the standard tools in the *NuSTARDAS* package. The cleaned level-2 event products were extracted using the `nupipeline` routine. The source photons were extracted using a circular region with a radius of $60''$ centered on the source, while the background events were extracted from an annulus region with an inner radius of $90''$ and an outer radius of $120''$. Finally, we used `nuproducts` to extract spectra and light curves for further analysis, and corrected the photon arrival times to the Solar System barycenter using the `barycorr` tool.

A.2. *Searches for periodic X-ray signals*

We searched for significant peaks in the power spectra extracted from the *NICER* and *NuSTAR* datasets over the whole energy range using the algorithm described by Israel & Stella (1996). This algorithm is based on a fast Fourier transform and accounts for non-Poissonian noise components in the Leahy-normalized (Leahy et al. 1983) power spectra. Our analysis did not reveal any significant peaks in any observations above a 3.5σ confidence threshold, calculated by considering the number of frequency trials examined. Focusing on the *NICER* datasets, the most stringent $3\text{-}\sigma$ upper limit on the flux pulsed fraction (which we define as the semi-amplitude of a sinusoidal modulation divided by the mean source count rate) was obtained from the second observation, the one with the longest exposure. This upper limit ranges between 6–10% for frequencies spanning 30–1000 Hz. For the *NuSTAR* data, after combining datasets from both FPMs, the upper limit is between 8–13% within the same frequency range.

We also searched for periodic signals in the second *NICER* observation and the *NuSTAR* observation using Fourier-domain acceleration search techniques. Specifically, we employed the `accelsearch` pipeline from the *PRESTO*⁸ pulsar timing software package (Ransom et al. 2002) to search for signals within the frequency range of 1–1000 Hz, summing up to eight harmonics. To account for potential power drifts in the Fourier domain, we allowed the powers of signals to drift by up to 200 frequency bins. Moreover, we conducted a “jerk” search, allowing the powers of the signals to drift by up to 600 frequency derivative bins, as described by Andersen & Ransom (2018). No promising signals were detected.

For *EP/FXT* observations, we also searched the pulsed signal using `powspec` and further checked the signal around the QPO frequency with the blind search technique developed by the Fermi-LAT collaboration (Atwood et al. 2006). No confirmed signals were detected, consistent with the result obtained from *NICER* and *NuSTAR* data. In the end, the upper limit for the FXT timing mode observation is between 6–13% for frequencies spanning 30–1000 Hz using the algorithm described by Israel & Stella (1996).

A.3. *Optical and infrared*

A.3.1. *GROND*

EP J182730.0-095633 was observed with the Gamma-ray Burst Optical Near-infrared Detector (GROND, Greiner et al. 2008); mounted at the MPG 2.2 m telescope at ESO’s La Silla observatory for six nights from September 7th to October 1st 2024 (see Table B.2). Observations were performed simultaneously in the g' , r' , i' , J , H , and K_s bands with typical exposures of 30 min per band and observation. The data were reduced using the standard IRAF-based GROND pipeline (Krühler et al. 2008). The photometry was calibrated against PanSTARSS DR1 (Chambers et al. 2016) (g' , r' , i') and the Two Micron All Sky Survey catalogue (2MASS; Skrutskie et al. 2006) (J , H , and K_s) and converted into the AB system.

A.3.2. *SVOM/VT*

The VT (Visible Telescope) is an optical telescope onboard the *Space Variable Objects Monitor mission* (SVOM, Wei et al. 2016). The effective aperture is 43 cm. The field of view is $26' \times 26'$, giving the pixel scale of $0.76''$. It conducts the observation with two broad-band channels VT_B and VT_R simultaneously, covering 400–650 nm and 650–1000 nm, respectively. Detailed information on VT can be referred to Qiu et al. (2025, in preparation). EP J182730.0-095633 was observed twice by VT during its commissioning phase via Target Of Opportunity (ToO) mode, one on 13:23:58 UT, 2024-09-06 and the other on 21:45:55 UT, 2024-09-28. The exposure time was set to be 20 s for single frame. All the data were processed in a standard manner, including zero correction, dark correction, and flat-field correction. After pre-processing, the images for each band obtained during each observation were stacked to increase the signal-to-noise ratio.

⁸ <https://github.com/scottransom/presto>

A.3.3. NOT

The optical photometry follow-up observation was carried out using the 2.56 m Nordic Optical Telescope (NOT; Roque de los Muchachos observatory, La Palma, Spain) equipped with Alhambra Faint Object Spectrograph and Camera (ALFOSC) at 20:42:54 UT on 2024-09-07, i.e. 3.4 days after the trigger, and 4×180 s frames were obtained in the SDSS-*r* band. The NOT data are reduced by standard procedures with the IMAGE REDUCTION AND ANALYSIS FACILITY (IRAF) v2.16 (Tody 1986), including bias subtraction, flat-field correction and images combination.

A.3.4. TRT

We began to observe EP J182730.0-095633 using the 0.7-m telescope of the Thai Robotic Telescope (TRT) network, located at Sierra Remote Observatories, USA. The observation started at 02:34:30 UT on 2024-09-08, i.e. 3.7 days after the trigger and several frames were obtained in the Johnson *B* band. Raw data were processed automatically using the TRT's standard data reduction pipeline. We stack clean science frames using IRAF to improve the signal-to-noise ratio.

A.3.5. ALT100C

ALT100C is a 1-meter telescope located at Altay observatory, Xinjiang, China. The observation of EP J182730.0-095633 was conducted at 14:49:20 UT on 2024-09-08, i.e. 4.2 days after the trigger in the *g*, *r* and *i* bands. The data are also reduced by IRAF and calibrated with nearby PanSTARRS stars.

A.3.6. TNT

The Tsinghua-NAOC Telescope (TNT, Huang et al. 2012), an 80-cm Cassegrain reflecting telescope located at Xinglong Observatory of the National Astronomical Observatories of China (NAOC), was used to observe the field of the X-ray transient EP J182730.0-095633. Observations were conducted in the *r* and *i* bands, obtaining 6×600 s exposures per band, with a median observation date of 2024-10-11T11:33:50. After the bias and flat-field correction, the images were stacked by the imcombine program in IRAF. The photometric measurements were carried out using the SOURCE EXTRACTOR (SEXTRACTOR, Bertin & Arnouts 1996). The automatic aperture photometry was derived from Kron's "first moment" algorithm (Kron 1980). The instrumental magnitude was then calibrated to Pan-STARR DR1.

A.3.7. Mephisto

The Multi-channel Photometric Survey Telescope (Mephisto⁹) is a wide-field ground based telescope with a 1.6-meter primary mirror featuring a field of view of 2 square degrees (Yuan et al. 2020). Observations were conducted at 16:11:28 UT on 2024-09-07, i.e. 3.2 days after the trigger, in the *v*, *r* and *z* bands. For data reduction, the raw frames were processed through a dedicated pre-processing pipeline developed for Mephisto. This pipeline includes bias subtraction, dark subtraction, flat fielding, and cosmic ray removal. Photometric calibration was performed using the Gaia BP/RP low-resolution spectra (XP spectra) of non-variable stars. Since there were no detections in either the single frames or the stacked frames for each band, we calculated the 5σ limiting magnitudes for each frame based on the image's Full Width at Half Maximum (FWHM) and the background fluctuations at the target's position.

A.4. Radio

A.4.1. ATCA

Two radio observations were carried out using the Australia Telescope Compact Array (ATCA) at 4 cm, one on September 12th, 2024 from 09:00 to 14:00 UT (Wang et al. 2024a), and the other on September 21st, 2024 from 07:30 to 12:30 UT. The ATCA observations were conducted as part of the project C3615 (PI: Yanan Wang). The central frequencies were set at 5.5 GHz and 9 GHz, each with a bandwidth of 2 GHz. These observations were coordinated with EP/FXT observations to investigate any correlations between the radio and X-ray emissions. Data were processed using the Common Astronomy Software Applications (CASA; McMullin et al. 2007; CASA Team et al. 2022) with standard interferometric imaging methods. Flux density and gain calibrators 1934-638 and 1829-106 were used for the calibration.

A.4.2. MeerKAT

We observed the position of EP J182730.0-095633 with the MeerKAT radio telescope (Camilo et al. 2018; Jonas 2018), as part of program SCI-20230907-JB-01 (PIs Bright & Carotenuto). We conducted three observations, each with the same total on-source time of 42 minutes. We observed quasi-simultaneously at L- and S-band, the first at a central frequency of 1.28 GHz and a

⁹ <http://www.mephisto.ynu.edu.cn/about/Mephisto>

total bandwidth of 856 MHz, and the second at 3.06 GHz (S-band, S4), with a total bandwidth of 875 MHz. The first observation started on September 21st 2024 at 15:16 UTC (L-band) and 16:51 UTC (S-band). The second observation was performed on October 21st 2024 at 13:45 UTC (S-band) and on October 22nd 2024 at 19:09 UTC (L-band), while the third observation was conducted on October 28th 2025 at 16:44 UTC (S-band) and 18:14 UTC (L-band). PKS J1939–6342 and PKS 1830–211 were used as flux and complex gain calibrators, respectively. The data were reduced with the `OxKAT` pipeline (Heywood 2020), which performs standard flagging, calibration and imaging using `tricolour` (Hugo et al. 2022), `CASA` and `WSCLEAN` (Offringa et al. 2014), respectively. In the imaging step, we adopted a Briggs weighting scheme with a -0.3 robust parameter. The typical values for the image rms-noise are $\sim 10 \mu\text{Jy beam}^{-1}$ at S-band and $20 \sim 30 \mu\text{Jy beam}^{-1}$ at L-band, due to the presence of diffuse emission in the field, stronger at lower frequencies.

B. SUPPLEMENTARY MATERIAL

In this section, we present the detailed results of the X-ray spectral fitting, optical and infrared follow-up observations and PSDs of *EP/FXT* and *NICER* during the X-ray outburst.

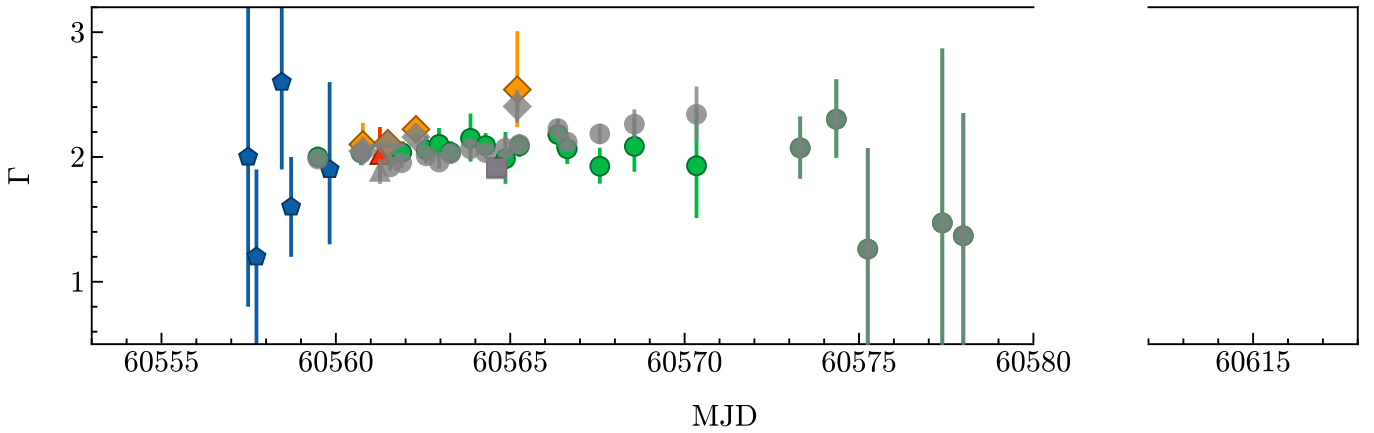


Figure B.1. Evolutionary trend of the photon index Γ using two different data analysis strategies for *EP/FXT*, *NICER*, *Swift/XRT* and *NuSTAR* data. The result shown as gray symbols is obtained by fixing the column density N_{H} to the typical parameter value of $3.1 \times 10^{22} \text{ cm}^{-2}$ during the outburst. The result obtained with variable column density (same as in Figure 3) is also plotted for comparison.

REFERENCES

- Alabarta, K., Altamirano, D., Méndez, M., et al. 2021, *MNRAS*, 507, 5507, doi: [10.1093/mnras/stab2241](https://doi.org/10.1093/mnras/stab2241)
- Altamirano, D., & Strohmayer, T. 2012, *ApJL*, 754, L23, doi: [10.1088/2041-8205/754/2/L23](https://doi.org/10.1088/2041-8205/754/2/L23)
- Andersen, B. C., & Ransom, S. M. 2018, *ApJL*, 863, L13, doi: [10.3847/2041-8213/aad59f](https://doi.org/10.3847/2041-8213/aad59f)
- Armas Padilla, M., Wijnands, R., Altamirano, D., et al. 2014, *MNRAS*, 439, 3908, doi: [10.1093/mnras/stu243](https://doi.org/10.1093/mnras/stu243)
- Arnaud, K. A. 1996, in *Astronomical Society of the Pacific Conference Series*, Vol. 101, *Astronomical Data Analysis Software and Systems V*, ed. G. H. Jacoby & J. Barnes, 17
- Atapin, K., Fabrika, S., & Caballero-García, M. D. 2019, *MNRAS*, 486, 2766, doi: [10.1093/mnras/stz1027](https://doi.org/10.1093/mnras/stz1027)
- Atwood, W. B., Ziegler, M., Johnson, R. P., & Baughman, B. M. 2006, *ApJL*, 652, L49, doi: [10.1086/510018](https://doi.org/10.1086/510018)
- Avakyan, A., Neumann, M., Zainab, A., et al. 2023, *A&A*, 675, A199, doi: [10.1051/0004-6361/202346522](https://doi.org/10.1051/0004-6361/202346522)
- Bahramian, A., & Degenaar, N. 2023, in *Handbook of X-ray and Gamma-ray Astrophysics*, 120, doi: [10.1007/978-981-16-4544-0_94-1](https://doi.org/10.1007/978-981-16-4544-0_94-1)
- Bahramian, A., & Rushton, A. 2022, *bersavosh/XRB-LrLx_pub*: update 20220908, v220908, Zenodo, doi: [10.5281/zenodo.7059313](https://doi.org/10.5281/zenodo.7059313)
- Banerjee, S., Gilfanov, M., Bhattacharyya, S., & Sunyaev, R. 2020, *MNRAS*, 498, 5353, doi: [10.1093/mnras/staa2788](https://doi.org/10.1093/mnras/staa2788)
- Barthelmy, S. D., Barbier, L. M., Cummings, J. R., et al. 2005, *SSRv*, 120, 143, doi: [10.1007/s11214-005-5096-3](https://doi.org/10.1007/s11214-005-5096-3)
- Belloni, T. 2010, *The Jet Paradigm*, Vol. 794, doi: [10.1007/978-3-540-76937-8](https://doi.org/10.1007/978-3-540-76937-8)
- Belloni, T., & Hasinger, G. 1990, *A&A*, 230, 103

Table B.1. X-ray spectral fitting results of EP J182730.0-095633.

Obs date	$T - T_0$ (day)	Instrument	OBSID	N_H (10^{22} cm^{-2})	Γ	$F_{\text{unabsorbed}, 0.5-10}$ ($\times 10^{-11} \text{ erg s}^{-1} \text{ cm}^{-2}$)	$\chi^2/\text{d.o.f.}$	Exposure (seconds)
2024-09-01/02/03	-1.8	EP/WXT	06800000061/63/68	3.1*	2.0*	< 4.3	...	27230
2024-09-04	0	EP/WXT	06800000067	3.1*	$2.0^{+1.3}_{-1.2}$	14^{+10}_{-5}	58.3/68	6075
	0.3	EP/WXT	08500000148	3.1*	$1.2^{+0.7}_{-0.7}$	37^{+16}_{-9}	99.8/104	9246
2024-09-05	1.0	EP/WXT	06800000071	3.1*	$2.6^{+0.7}_{-0.7}$	52^{+29}_{-15}	50.1/47	2987
	1.3	EP/WXT	06800000069	3.1*	$1.6^{+0.4}_{-0.4}$	40^{+7}_{-6}	130.5/146	9155
2024-09-06	2.1	EP/FXT	06800000074	$3.1^{+0.1}_{-0.1}$	$2.00^{+0.08}_{-0.08}$	35^{+2}_{-2}	307.8/297	5966
	2.4	EP/WXT	06800000070	3.1*	$1.9^{+0.7}_{-0.6}$	30^{+8}_{-7}	129.5/94	6070
2024-09-07	3.3	EP/FXT	06800000081	$3.3^{+0.2}_{-0.2}$	$2.03^{+0.10}_{-0.10}$	23^{+2}_{-1}	195.6/189	2983
	3.3	NICER/XTI	7204880101	$3.2^{+0.2}_{-0.2}$	$2.1^{+0.14}_{-0.17}$	27^{+3}_{-2}	109.39/117	223
2024-09-08	3.8	Swift/XRT	00016796001	$3.4^{+0.5}_{-0.5}$	$2.02^{+0.22}_{-0.21}$	20^{+4}_{-3}	61.5/50	2864
	4.1	NICER/XTI	7204880102	$3.1^{+0.1}_{-0.1}$	$2.11^{+0.06}_{-0.04}$	$25.3^{+0.7}_{-0.6}$	607.69/603	3921
	4.1	EP/FXT	06800000079	$3.3^{+0.1}_{-0.1}$	$2.01^{+0.07}_{-0.07}$	$21.0^{+1.0}_{-0.9}$	303.7/276	5941
	4.5	EP/FXT	06800000080	$3.3^{+0.2}_{-0.1}$	$2.04^{+0.09}_{-0.09}$	20^{+1}_{-1}	221.8/209	3935
2024-09-09	5.2	EP/FXT	06800000082	$3.2^{+0.2}_{-0.2}$	$2.06^{+0.11}_{-0.11}$	18^{+1}_{-1}	145.3/151	2984
	5.5	EP/FXT	06800000083	$3.4^{+0.2}_{-0.2}$	$2.10^{+0.13}_{-0.13}$	17^{+2}_{-1}	154.8/128	2716
	4.9	NICER/XTI	7204880103	$3.2^{+0.1}_{-0.1}$	$2.22^{+0.08}_{-0.08}$	24^{+1}_{-1}	527.82/515	1543
2024-09-10	5.9	EP/FXT	06800000087	$3.1^{+0.2}_{-0.2}$	$2.04^{+0.09}_{-0.09}$	$14.9^{+0.9}_{-0.8}$	231.7/218	5319
	6.4	EP/FXT	06800000088	$3.3^{+0.3}_{-0.3}$	$2.15^{+0.20}_{-0.19}$	14^{+2}_{-2}	75.5/64	1580
2024-09-11	6.9	EP/FXT	06800000089	$3.2^{+0.2}_{-0.2}$	$2.09^{+0.10}_{-0.10}$	$12.8^{+0.9}_{-0.7}$	188.4/185	5361
	7.2	NuSTAR	91001334002	3.7 ± 1.3	1.92 ± 0.03	8.2 ± 0.3	718.7/765	2690
	7.4	EP/FXT	06800000090	$2.9^{+0.4}_{-0.3}$	$2.00^{+0.21}_{-0.20}$	11^{+2}_{-1}	82.5/57	1500
2024-09-12	7.8	NICER/XTI	7204880105	$3.3^{+0.6}_{-0.4}$	$2.54^{+0.47}_{-0.30}$	15^{+6}_{-3}	168.8/165	703
	7.8	EP/FXT	06800000091	$3.1^{+0.2}_{-0.1}$	$2.09^{+0.09}_{-0.09}$	$10.7^{+0.7}_{-0.6}$	240.7/221	7581
2024-09-13	8.9	EP/FXT	06800000095	$3.0^{+0.2}_{-0.2}$	$2.18^{+0.12}_{-0.12}$	$7.6^{+0.7}_{-0.6}$	132.5/133	5886
	9.2	EP/FXT	06800000096	$3.0^{+0.2}_{-0.2}$	$2.07^{+0.13}_{-0.12}$	$6.8^{+0.6}_{-0.5}$	144.3/124	5976
2024-09-14	10.1	EP/FXT	06800000097	$2.6^{+0.2}_{-0.2}$	$1.93^{+0.15}_{-0.14}$	$4.5^{+0.4}_{-0.3}$	118.1/97	5978
2024-09-15	11.1	EP/FXT	06800000098	$2.8^{+0.3}_{-0.3}$	$2.08^{+0.22}_{-0.20}$	$3.3^{+0.5}_{-0.3}$	39.9/48	4091
2024-09-17	12.9	EP/FXT	06800000110	$2.4^{+0.7}_{-0.6}$	$1.93^{+0.47}_{-0.42}$	$1.5^{+0.5}_{-0.2}$	19.4/16	2992
2024-09-20	15.9	EP/FXT	06800000111	3.1*	$2.07^{+0.25}_{-0.25}$	$0.49^{+0.06}_{-0.05}$	132.7/114	5987
2024-09-21	16.9	EP/FXT	06800000114	3.1*	$2.30^{+0.32}_{-0.31}$	$0.24^{+0.04}_{-0.03}$	100.1/85	8979
2024-09-22	17.8	EP/FXT	06800000117	3.1*	$1.26^{+0.81}_{-0.81}$	$0.059^{+0.003}_{-0.002}$	11.4/17	5960
2024-09-23	19.4	EP/FXT	06800000118	3.1*	2.0*	< 0.068	...	1387
2024-09-24	20.0	EP/FXT	06800000120	3.1*	$1.47^{+1.40}_{-1.40}$	$0.043^{+0.045}_{-0.018}$	10.8/14	5842
	20.6	EP/FXT	06800000123	3.1*	$1.37^{+0.98}_{-0.98}$	$0.030^{+0.020}_{-0.012}$	13.5/12	8095
2024-11-01	57.9	Swift/XRT	00016796002	3.1*	2.0*	< 0.037	...	2582

NOTE— T_0 is set as the starting time of the WXT observation during which the source was firstly detected, at 2024-09-04T10:12:56 (UTC). The parameters marked with an asterisk were held fixed at the quoted values in the fits.

Table B.2. Optical and infrared follow-up observations of EP J182730.0-095633.

Obs date	$T - T_0$ (day)	Instrument	Filter	Detection	Observed magnitude or 5σ upper limit
2024-09-06	2.1	SVOM/VT	VT_R, VT_B	N	$> 21.4 / > 22.9$
2024-09-07	2.6	GROND	J, H, K_s	Y	$17.97 \pm 0.22^J / 16.73 \pm 0.13^H / 16.32 \pm 0.13^K$
			g', r', i'	N	$> 23.9^g / > 22.6^r / > 21.5^i$
		Mephisto	v, r, z	N	$> 20.7^v / > 20.5^r / > 19.36^z$
2024-09-08	3.2	Mephisto	v, r, z	N	$> 20.7^v / > 20.5^r / > 19.36^z$
	3.4	NOT	r	Y	23.87 ± 0.35^r
	3.6	GROND	J, H, K_s	Y	$18.09 \pm 0.18^J / 16.81 \pm 0.18^H / 16.43 \pm 0.16^K$
			g', r', i'	Y	$> 23.9^g / 23.86 \pm 0.30^r / 21.77 \pm 0.10^i$
	3.7	TRT	B	N	$> 21.4^B$
4.2	ALT100C	r, g, i	N	$> 22.3^r / > 21.7^g / > 20.9^i$	
2024-09-09	4.6	GROND	J, H, K_s	Y	$18.01 \pm 0.18^J / 16.93 \pm 0.16^H / 16.50 \pm 0.15^K$
			g', r', i'	Y	$> 23.6^g / > 23.2^r / 21.95 \pm 0.15^i$
2024-09-11	6.7	GROND	J, H, K_s	N	- / - / -
			g', r', i'	N	$> 21.2^g / > 21.5^r / > 20.7^i$
2024-09-18	13.7	GROND	J, H, K_s	N	$> 19.2^g / > 17.7^r / > 17.4^i$
			g', r', i'	N	$> 21.7^g / > 22.3^r / > 21.6^i$
2024-09-28	24.5	SVOM/VT	VT_R, VT_B	N	$> 21.6 / > 22.3$
2024-10-01	27.6	GROND	J, H, K_s	N	- / - / -
			g', r', i'	N	$> 21.0^g / > 21.2^r / > 21.0^i$
2024-10-11	37.0	TNT	r, i	N	$> 18.24^r / > 17.54^i$

NOTE— T_0 is set as the starting time of the WXT observation during which the source was firstly detected, at 2024-09-04T10:12:56 (UTC).

With poor seeing conditions during the GROND observations in the J , H , and K bands on September 11th and October 1st, it was not feasible to accurately constrain the flux of the source due to its proximity to other brighter sources. As a result, the magnitudes in these bands are not provided.

Table B.3. Radio follow-up observations of EP J182730.0-095633.

Obs date	$T - T_0$ (day)	Instrument	Filter	Detection	Peak flux density / 3σ upper limit $\mu\text{Jy}/\text{beam}$
2024-09-12	7.9	ATCA	5.5 GHz	Y	101.2 ± 5.4
	7.9	ATCA	9 GHz	Y	126.3 ± 5.2
2024-09-21	16.9	ATCA	5.5 GHz	N	< 57
	16.9	ATCA	9 GHz	N	< 60
	17.2	MeerKAT	1.28 GHz (L-band)	N	< 69
	17.3	MeerKAT	3.06 GHz (S-band)	Y	33 ± 4
2024-10-21	47.1	MeerKAT	3.06 GHz (S-band)	N	< 36
2024-10-21	48.4	MeerKAT	1.28 GHz (L-band)	Y	58 ± 12
2024-10-22	54.3	MeerKAT	3.06 GHz (S-band)	N	< 36
2024-10-22	54.3	MeerKAT	1.28 GHz (L-band)	N	< 105

NOTE— T_0 is set as the starting time of the WXT observation during which the source was firstly detected, at 2024-09-04T10:12:56 (UTC).

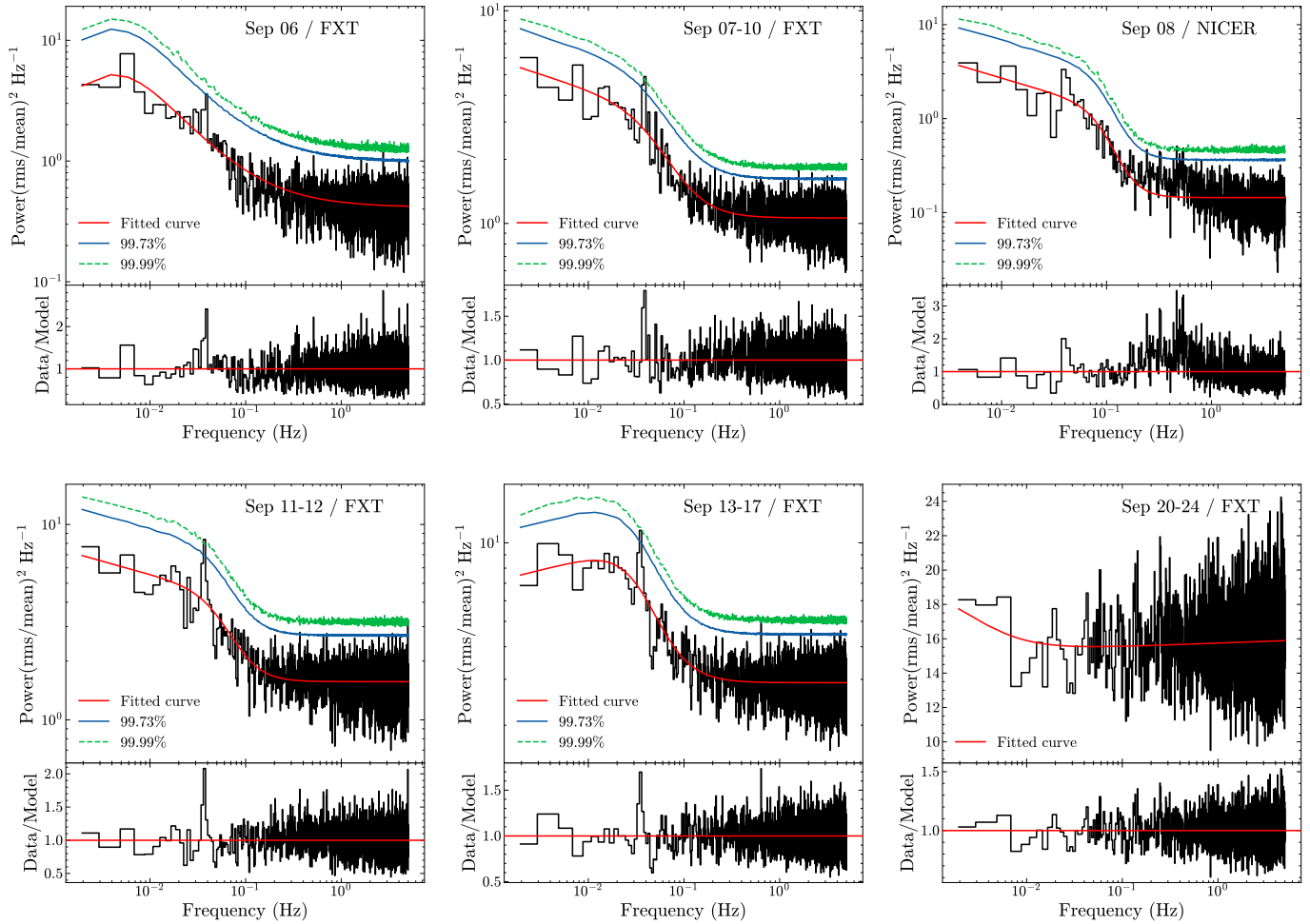


Figure B.2. PSDs of *EP/FXT* and *NICER* during the outburst. The centroid frequency of the most prominent QPO holds steady at ~ 0.04 Hz. For the *EP/FXTA* (TM mode) data, we combined them to improve the signal-to-noise ratio. The absence of the QPO signal in the final FXT dataset (from September 20th to 24th) is likely attributed to the extremely low count rate of the source during this period.

Belloni, T. M., Motta, S. E., & Muñoz-Darias, T. 2011, *Bulletin of the Astronomical Society of India*, 39, 409, doi: [10.48550/arXiv.1109.3388](https://doi.org/10.48550/arXiv.1109.3388)

Benz, A. O., & Güdel, M. 2010, *ARA&A*, 48, 241, doi: [10.1146/annurev-astro-082708-101757](https://doi.org/10.1146/annurev-astro-082708-101757)

Beri, A., Gaur, V., Charles, P., et al. 2023, *MNRAS*, 522, 4598, doi: [10.1093/mnras/stad1277](https://doi.org/10.1093/mnras/stad1277)

Bertin, E., & Arnouts, S. 1996, *A&AS*, 117, 393, doi: [10.1051/aas:1996164](https://doi.org/10.1051/aas:1996164)

Bloom, J. S., Giannios, D., Metzger, B. D., et al. 2011, *Science*, 333, 203, doi: [10.1126/science.1207150](https://doi.org/10.1126/science.1207150)

Bozzo, E., Papitto, A., Ferrigno, C., & Belloni, T. M. 2014, *A&A*, 570, L2, doi: [10.1051/0004-6361/201424788](https://doi.org/10.1051/0004-6361/201424788)

Bozzo, E., Ferrigno, C., Stevens, J., et al. 2011, *A&A*, 535, L1, doi: [10.1051/0004-6361/201118022](https://doi.org/10.1051/0004-6361/201118022)

Brandt, S., Lund, N., & Rao, A. R. 1990, *Advances in Space Research*, 10, 239, doi: [10.1016/0273-1177\(90\)90148-S](https://doi.org/10.1016/0273-1177(90)90148-S)

Brown, G. E., & Bethe, H. A. 1994, *ApJ*, 423, 659, doi: [10.1086/173844](https://doi.org/10.1086/173844)

Buisson, D. J. K., Fabian, A. C., Barret, D., et al. 2019, *MNRAS*, 490, 1350, doi: [10.1093/mnras/stz2681](https://doi.org/10.1093/mnras/stz2681)

Burke, M. J., Gilfanov, M., & Sunyaev, R. 2017, *MNRAS*, 466, 194, doi: [10.1093/mnras/stw2514](https://doi.org/10.1093/mnras/stw2514)

Burrows, D. N., Kennea, J. A., Ghisellini, G., et al. 2011, *Nature*, 476, 421, doi: [10.1038/nature10374](https://doi.org/10.1038/nature10374)

Camilo, F., Scholz, P., Serylak, M., et al. 2018, *ApJ*, 856, 180, doi: [10.3847/1538-4357/aab35a](https://doi.org/10.3847/1538-4357/aab35a)

Cardelli, J. A., Clayton, G. C., & Mathis, J. S. 1989, *ApJ*, 345, 245, doi: [10.1086/167900](https://doi.org/10.1086/167900)

CASA Team, Bean, B., Bhatnagar, S., et al. 2022, *PASP*, 134, 114501, doi: [10.1088/1538-3873/ac9642](https://doi.org/10.1088/1538-3873/ac9642)

Casella, P., Belloni, T., Homan, J., & Stella, L. 2004, *A&A*, 426, 587, doi: [10.1051/0004-6361:20041231](https://doi.org/10.1051/0004-6361:20041231)

Cash, W. 1979, *ApJ*, 228, 939, doi: [10.1086/156922](https://doi.org/10.1086/156922)

Chambers, K. C., Magnier, E. A., Metcalfe, N., et al. 2016, *arXiv e-prints*, arXiv:1612.05560, doi: [10.48550/arXiv.1612.05560](https://doi.org/10.48550/arXiv.1612.05560)

Chen, W., Shrader, C. R., & Livio, M. 1997, *ApJ*, 491, 312, doi: [10.1086/304921](https://doi.org/10.1086/304921)

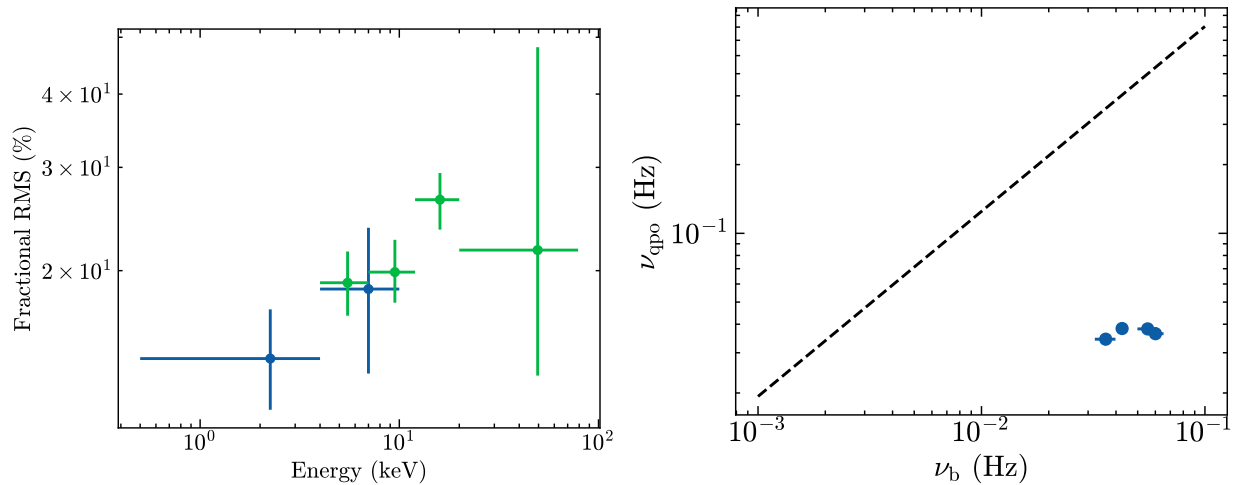


Figure B.3. Left panel: the RMS spectrum calculated using the same data set as Figure 2 (*EP/FXT+NuSTAR* on September 11th, 2024). The blue dots are from *EP-FXT* and green dots from *NuSTAR*. Right panel: the relation between the low frequency break (ν_b) of the PSD and the centroid frequency of the QPO signal (ν_{qpo}), with the results of EP J182730.0-095633 denoted as blue circles. Here we use the PSDs from Sep 07–10 (FXT), Sep 11 (NuSTAR), Sep 11–12 (FXT), and Sep 13–17 (FXT), where the QPO significance exceeds 3σ . The black dashed line is the empirical W-K relation between the two variables for type-C LFQPOs. ν_{qpo} are 38.2 ± 0.2 , 38.3 ± 0.3 , 36.4 ± 0.4 , and 34.4 ± 0.4 mHz for the four PSDs, respectively, while ν_b are 55 ± 6 , 43 ± 2 , 60 ± 5 , and 36 ± 4 mHz.

Chen, Y., Cui, W., Han, D., et al. 2020, in Society of Photo-Optical Instrumentation Engineers (SPIE) Conference Series, Vol. 11444, Space Telescopes and Instrumentation 2020: Ultraviolet to Gamma Ray, ed. J.-W. A. den Herder, S. Nikzad, & K. Nakazawa, 114445B, doi: [10.1117/12.2562311](https://doi.org/10.1117/12.2562311)

Cheng, H., Ling, Z., Zhang, C., et al. 2024a, *Experimental Astronomy*, 57, 10, doi: [10.1007/s10686-024-09932-0](https://doi.org/10.1007/s10686-024-09932-0)

Cheng, H., Zhang, C., Ling, Z., et al. 2025, arXiv e-prints, arXiv:2505.18939. <https://arxiv.org/abs/2505.18939>

Cheng, H. Q., Wen, S. X., Wang, Y., et al. 2024b, *The Astronomer's Telegram*, 16805, 1

Corbel, S., et al. 2013, *MNRAS*, 428, 2500, doi: [10.1093/mnras/sts215](https://doi.org/10.1093/mnras/sts215)

Corral-Santana, J. M., Casares, J., Muñoz-Darias, T., et al. 2016, *A&A*, 587, A61, doi: [10.1051/0004-6361/201527130](https://doi.org/10.1051/0004-6361/201527130)

—. 2013, *Science*, 339, 1048, doi: [10.1126/science.1228222](https://doi.org/10.1126/science.1228222)

Degenaar, N., & Wijnands, R. 2009, *A&A*, 495, 547, doi: [10.1051/0004-6361:200810654](https://doi.org/10.1051/0004-6361:200810654)

Del Santo, M., Nucita, A. A., Lodato, G., et al. 2014, *MNRAS*, 444, 93, doi: [10.1093/mnras/stu1436](https://doi.org/10.1093/mnras/stu1436)

Dewangan, G. C., Titarchuk, L., & Griffiths, R. E. 2006, *ApJL*, 637, L21, doi: [10.1086/499235](https://doi.org/10.1086/499235)

Díaz Trigo, M., Altamirano, D., Dinçer, T., et al. 2018, *A&A*, 616, A23, doi: [10.1051/0004-6361/201832693](https://doi.org/10.1051/0004-6361/201832693)

Drlica-Wagner, A., Bechtol, K., Mau, S., et al. 2020, *ApJ*, 893, 47, doi: [10.3847/1538-4357/ab7eb9](https://doi.org/10.3847/1538-4357/ab7eb9)

Dubus, G., Hameury, J. M., & Lasota, J. P. 2001, *A&A*, 373, 251, doi: [10.1051/0004-6361:20010632](https://doi.org/10.1051/0004-6361:20010632)

El Byad, H., Bachetti, M., Columbu, S., et al. 2025, arXiv e-prints, arXiv:2505.16921, doi: [10.48550/arXiv.2505.16921](https://doi.org/10.48550/arXiv.2505.16921)

Evans, P. A., Beardmore, A. P., Page, K. L., et al. 2009, *MNRAS*, 397, 1177, doi: [10.1111/j.1365-2966.2009.14913.x](https://doi.org/10.1111/j.1365-2966.2009.14913.x)

Evans, P. A., Page, K. L., Osborne, J. P., et al. 2020, *ApJS*, 247, 54, doi: [10.3847/1538-4365/ab7db9](https://doi.org/10.3847/1538-4365/ab7db9)

Fu, S. Y., An, J., Jiang, S. Q., et al. 2024, *The Astronomer's Telegram*, 16807, 1

Gehrels, N., Chincarini, G., Giommi, P., et al. 2004, *ApJ*, 611, 1005, doi: [10.1086/422091](https://doi.org/10.1086/422091)

Gendreau, K. C., Arzoumanian, Z., Adkins, P. W., et al. 2016, in Society of Photo-Optical Instrumentation Engineers (SPIE) Conference Series, Vol. 9905, Space Telescopes and Instrumentation 2016: Ultraviolet to Gamma Ray, ed. J.-W. A. den Herder, T. Takahashi, & M. Bautz, 99051H, doi: [10.1117/12.2231304](https://doi.org/10.1117/12.2231304)

Greiner, J., Bornemann, W., Clemens, C., et al. 2008, *PASP*, 120, 405, doi: [10.1086/587032](https://doi.org/10.1086/587032)

Grimm, H. J., Gilfanov, M., & Sunyaev, R. 2002, *A&A*, 391, 923, doi: [10.1051/0004-6361:20020826](https://doi.org/10.1051/0004-6361:20020826)

Hailey, C. J., Mori, K., Bauer, F. E., et al. 2018, *Nature*, 556, 70, doi: [10.1038/nature25029](https://doi.org/10.1038/nature25029)

Hands, A. D. P., Warwick, R. S., Watson, M. G., & Helfand, D. J. 2004, *MNRAS*, 351, 31, doi: [10.1111/j.1365-2966.2004.07777.x](https://doi.org/10.1111/j.1365-2966.2004.07777.x)

Harrison, F. A., Craig, W. W., Christensen, F. E., et al. 2013, *ApJ*, 770, 103, doi: [10.1088/0004-637X/770/2/103](https://doi.org/10.1088/0004-637X/770/2/103)

Heinke, C. O., Bahramian, A., Degenaar, N., & Wijnands, R. 2015, *MNRAS*, 447, 3034, doi: [10.1093/mnras/stu2652](https://doi.org/10.1093/mnras/stu2652)

Heywood, I. 2020, oxkat: Semi-automated imaging of MeerKAT observations, Astrophysics Source Code Library, record ascl:2009.003

- HI4PI Collaboration, Ben Bekhti, N., Flöer, L., et al. 2016, *A&A*, 594, A116, doi: [10.1051/0004-6361/201629178](https://doi.org/10.1051/0004-6361/201629178)
- Huang, F., Li, J.-Z., Wang, X.-F., et al. 2012, *Research in Astronomy and Astrophysics*, 12, 1585, doi: [10.1088/1674-4527/12/11/012](https://doi.org/10.1088/1674-4527/12/11/012)
- Hugo, B. V., Perkins, S., Merry, B., Mauch, T., & Smirnov, O. M. 2022, in *Astronomical Society of the Pacific Conference Series*, Vol. 532, *Astronomical Society of the Pacific Conference Series*, ed. J. E. Ruiz, F. Pierfederici, & P. Teuben, 541, doi: [10.48550/arXiv.2206.09179](https://doi.org/10.48550/arXiv.2206.09179)
- Hunter, J. D. 2007, *Computing in Science and Engineering*, 9, 90, doi: [10.1109/MCSE.2007.55](https://doi.org/10.1109/MCSE.2007.55)
- Ichimaru, S. 1977, *ApJ*, 214, 840, doi: [10.1086/155314](https://doi.org/10.1086/155314)
- Ingram, A. R., & Motta, S. E. 2019, *NewAR*, 85, 101524, doi: [10.1016/j.newar.2020.101524](https://doi.org/10.1016/j.newar.2020.101524)
- Israel, G. L., & Stella, L. 1996, *ApJ*, 468, 369, doi: [10.1086/177697](https://doi.org/10.1086/177697)
- Jonas, J. 2018, in *Proceedings of MeerKAT Science: On the Pathway to the SKA — PoS(MeerKAT2016)*, Vol. 277, 001, doi: [10.22323/1.277.0001](https://doi.org/10.22323/1.277.0001)
- Kalemci, E., Kara, E., & Tomsick, J. A. 2022, in *Handbook of X-ray and Gamma-ray Astrophysics*, ed. C. Bambi & A. Sanganello, 9, doi: [10.1007/978-981-16-4544-0_100-1](https://doi.org/10.1007/978-981-16-4544-0_100-1)
- King, A. R., & Ritter, H. 1998, *MNRAS*, 293, L42, doi: [10.1046/j.1365-8711.1998.01295.x](https://doi.org/10.1046/j.1365-8711.1998.01295.x)
- Kron, R. G. 1980, *ApJS*, 43, 305, doi: [10.1086/190669](https://doi.org/10.1086/190669)
- Krühler, T., Küpcü Yoldaş, A., Greiner, J., et al. 2008, *ApJ*, 685, 376, doi: [10.1086/590240](https://doi.org/10.1086/590240)
- Kuulkers, E., Ferrigno, C., Kretschmar, P., et al. 2021, *NewAR*, 93, 101629, doi: [10.1016/j.newar.2021.101629](https://doi.org/10.1016/j.newar.2021.101629)
- Leahy, D. A., Elsner, R. F., & Weisskopf, M. C. 1983, *ApJ*, 272, 256, doi: [10.1086/161288](https://doi.org/10.1086/161288)
- Levan, A. J., Tanvir, N. R., Brown, G. C., et al. 2016, *ApJ*, 819, 51, doi: [10.3847/0004-637X/819/1/51](https://doi.org/10.3847/0004-637X/819/1/51)
- Levine, A. M., Bradt, H., Cui, W., et al. 1996, *ApJL*, 469, L33, doi: [10.1086/310260](https://doi.org/10.1086/310260)
- Lewin, W. H. G., van Paradijs, J., & van den Heuvel, E. P. J., eds. 1995, *X-ray binaries*
- Li, T. P., & Ma, Y. Q. 1983, *ApJ*, 272, 317, doi: [10.1086/161295](https://doi.org/10.1086/161295)
- Li, Y., Yan, Z., Gao, C., & Yu, W. 2025, *MNRAS*, 538, 1143, doi: [10.1093/mnras/staf354](https://doi.org/10.1093/mnras/staf354)
- Lyu, M., Zhang, G., Méndez, M., et al. 2020, *ApJ*, 895, 120, doi: [10.3847/1538-4357/ab8cbe](https://doi.org/10.3847/1538-4357/ab8cbe)
- Mancuso, G. C., Altamirano, D., García, F., et al. 2019, *MNRAS*, 486, L74, doi: [10.1093/mnras/rlz057](https://doi.org/10.1093/mnras/rlz057)
- Mancuso, G. C., Altamirano, D., Bult, P., et al. 2023, *MNRAS*, 521, 5616, doi: [10.1093/mnras/stad949](https://doi.org/10.1093/mnras/stad949)
- Matsuoka, M., Kawasaki, K., Ueno, S., et al. 2009, *PASJ*, 61, 999, doi: [10.1093/pasj/61.5.999](https://doi.org/10.1093/pasj/61.5.999)
- McMullin, J. P., Waters, B., Schiebel, D., Young, W., & Golap, K. 2007, in *Astronomical Society of the Pacific Conference Series*, Vol. 376, *Astronomical Data Analysis Software and Systems XVI*, ed. R. A. Shaw, F. Hill, & D. J. Bell, 127
- Meier, D. L. 2012, *Black Hole Astrophysics: The Engine Paradigm*, doi: [10.1007/978-3-642-01936-4](https://doi.org/10.1007/978-3-642-01936-4)
- Motta, S., Muñoz-Darias, T., Casella, P., Belloni, T., & Homan, J. 2011, *MNRAS*, 418, 2292, doi: [10.1111/j.1365-2966.2011.19566.x](https://doi.org/10.1111/j.1365-2966.2011.19566.x)
- Muno, M. P., Lu, J. R., Baganoff, F. K., et al. 2005a, *ApJ*, 633, 228, doi: [10.1086/444586](https://doi.org/10.1086/444586)
- Muno, M. P., Pfahl, E., Baganoff, F. K., et al. 2005b, *ApJL*, 622, L113, doi: [10.1086/429721](https://doi.org/10.1086/429721)
- Narayan, R., & Yi, I. 1994, *ApJL*, 428, L13, doi: [10.1086/187381](https://doi.org/10.1086/187381)
- . 1995a, *ApJ*, 452, 710, doi: [10.1086/176343](https://doi.org/10.1086/176343)
- . 1995b, *ApJ*, 444, 231, doi: [10.1086/175599](https://doi.org/10.1086/175599)
- Nasa High Energy Astrophysics Science Archive Research Center (Heasarc). 2014, HEASoft: Unified Release of FTOOLS and XANADU, Astrophysics Source Code Library, record ascl:1408.004
- Offringa, A. R., McKinley, B., Hurley-Walker, N., et al. 2014, *MNRAS*, 444, 606, doi: [10.1093/mnras/stu1368](https://doi.org/10.1093/mnras/stu1368)
- Pasham, D. R., Cenko, S. B., Levan, A. J., et al. 2015, *ApJ*, 805, 68, doi: [10.1088/0004-637X/805/1/68](https://doi.org/10.1088/0004-637X/805/1/68)
- Pecaut, M. J., & Mamajek, E. E. 2013, *ApJS*, 208, 9, doi: [10.1088/0067-0049/208/1/9](https://doi.org/10.1088/0067-0049/208/1/9)
- Pecaut, M. J., Mamajek, E. E., & Bubar, E. J. 2012, *ApJ*, 746, 154, doi: [10.1088/0004-637X/746/2/154](https://doi.org/10.1088/0004-637X/746/2/154)
- Plotkin, R. M., Gallo, E., & Jonker, P. G. 2013, *ApJ*, 773, 59, doi: [10.1088/0004-637X/773/1/59](https://doi.org/10.1088/0004-637X/773/1/59)
- Porquet, D., Grosso, N., Burwitz, V., et al. 2005, *A&A*, 430, L9, doi: [10.1051/0004-6361:200400117](https://doi.org/10.1051/0004-6361:200400117)
- Qiao, E., & Liu, B. F. 2020, *MNRAS*, 496, 2704, doi: [10.1093/mnras/staa1671](https://doi.org/10.1093/mnras/staa1671)
- Ransom, S. M., Eikenberry, S. S., & Middleditch, J. 2002, *AJ*, 124, 1788, doi: [10.1086/342285](https://doi.org/10.1086/342285)
- Remillard, R. A., & McClintock, J. E. 2006, *ARA&A*, 44, 49, doi: [10.1146/annurev.astro.44.051905.092532](https://doi.org/10.1146/annurev.astro.44.051905.092532)
- Revnivtsev, M., Churazov, E., Gilfanov, M., & Sunyaev, R. 2001, *A&A*, 372, 138, doi: [10.1051/0004-6361:20010434](https://doi.org/10.1051/0004-6361:20010434)
- Revnivtsev, M., Sunyaev, R., & Borozdin, K. 2000, *A&A*, 361, L37, doi: [10.48550/arXiv.astro-ph/0005212](https://doi.org/10.48550/arXiv.astro-ph/0005212)
- Rodriguez, J., Corbel, S., Hannikainen, D. C., et al. 2004, *ApJ*, 615, 416, doi: [10.1086/423978](https://doi.org/10.1086/423978)
- Russell, D. M., Fender, R. P., Hynes, R. I., et al. 2006, *MNRAS*, 371, 1334, doi: [10.1111/j.1365-2966.2006.10756.x](https://doi.org/10.1111/j.1365-2966.2006.10756.x)
- Sakano, M., Warwick, R. S., Decourchelle, A., & Wang, Q. D. 2005, *MNRAS*, 357, 1211, doi: [10.1111/j.1365-2966.2005.08717.x](https://doi.org/10.1111/j.1365-2966.2005.08717.x)

- Schlafly, E. F., & Finkbeiner, D. P. 2011, *ApJ*, 737, 103, doi: [10.1088/0004-637X/737/2/103](https://doi.org/10.1088/0004-637X/737/2/103)
- Shakura, N. I., & Sunyaev, R. A. 1973, *A&A*, 24, 337
- Skrutskie, M. F., Cutri, R. M., Stiening, R., et al. 2006, *AJ*, 131, 1163, doi: [10.1086/498708](https://doi.org/10.1086/498708)
- Stoop, M., van den Eijnden, J., Degenaar, N., et al. 2021, *MNRAS*, 507, 330, doi: [10.1093/mnras/stab2127](https://doi.org/10.1093/mnras/stab2127)
- Strohmayer, T. E., & Smith, E. A. 2011, *The Astronomer's Telegram*, 3258, 1
- Swank, J., & Markwardt, C. 2001, in *Astronomical Society of the Pacific Conference Series*, Vol. 251, *New Century of X-ray Astronomy*, ed. H. Inoue & H. Kunieda, 94, doi: [10.48550/arXiv.astro-ph/0109240](https://doi.org/10.48550/arXiv.astro-ph/0109240)
- Tetarenko, B. E., Sivakoff, G. R., Heinke, C. O., & Gladstone, J. C. 2016, *ApJS*, 222, 15, doi: [10.3847/0067-0049/222/2/15](https://doi.org/10.3847/0067-0049/222/2/15)
- Timmer, J., & König, M. 1995, *A&A*, 300, 707
- Timmes, F. X., Woosley, S. E., & Weaver, T. A. 1996, *ApJ*, 457, 834, doi: [10.1086/176778](https://doi.org/10.1086/176778)
- Tody, D. 1986, in *Society of Photo-Optical Instrumentation Engineers (SPIE) Conference Series*, Vol. 627, *Instrumentation in astronomy VI*, ed. D. L. Crawford, 733, doi: [10.1117/12.968154](https://doi.org/10.1117/12.968154)
- Tse, K., Galloway, D. K., & Heger, A. 2023, arXiv e-prints, arXiv:2309.05236, doi: [10.48550/arXiv.2309.05236](https://doi.org/10.48550/arXiv.2309.05236)
- Ubertini, P., Lebrun, F., Di Cocco, G., et al. 2003, *A&A*, 411, L131, doi: [10.1051/0004-6361:20031224](https://doi.org/10.1051/0004-6361:20031224)
- van den Heuvel, E. P. J. 1992, in *NATO Advanced Study Institute (ASI) Series C*, Vol. 377, *X-Ray Binaries and Recycled Pulsars*, ed. E. P. J. van den Heuvel & S. A. Rappaport, 233–256
- van Paradijs, J. 1995, in *X-ray Binaries*, ed. W. H. G. Lewin, J. van Paradijs, & E. P. J. van den Heuvel, 536–577
- Verner, D. A., Ferland, G. J., Korista, K. T., & Yakovlev, D. G. 1996, *ApJ*, 465, 487, doi: [10.1086/177435](https://doi.org/10.1086/177435)
- Villa, G., Page, C. G., Turner, M. J. L., et al. 1976, *MNRAS*, 176, 609, doi: [10.1093/mnras/176.3.609](https://doi.org/10.1093/mnras/176.3.609)
- Wagner, R. M., Foltz, C. B., Shahbaz, T., et al. 2001, *ApJ*, 556, 42, doi: [10.1086/321572](https://doi.org/10.1086/321572)
- Walter, R., Bodaghee, A., Barlow, E. J., et al. 2004, *The Astronomer's Telegram*, 229, 1
- Wang, A., Feng, H., An, T., et al. 2024a, *The Astronomer's Telegram*, 16817, 1
- Wang, X.-L., Yan, Z., Xie, F.-G., Wang, J.-F., & Ma, R.-Y. 2024b, *ApJ*, 969, 152, doi: [10.3847/1538-4357/ad58d1](https://doi.org/10.3847/1538-4357/ad58d1)
- Wei, J., Cordier, B., Antier, S., et al. 2016, arXiv e-prints, arXiv:1610.06892, doi: [10.48550/arXiv.1610.06892](https://doi.org/10.48550/arXiv.1610.06892)
- Weng, S.-S., & Zhang, S.-N. 2015, *MNRAS*, 447, 486, doi: [10.1093/mnras/stu2610](https://doi.org/10.1093/mnras/stu2610)
- Wijnands, R., Degenaar, N., Armas Padilla, M., et al. 2015, *MNRAS*, 454, 1371, doi: [10.1093/mnras/stv1974](https://doi.org/10.1093/mnras/stv1974)
- Wijnands, R., & van der Klis, M. 1999, *ApJ*, 514, 939, doi: [10.1086/306993](https://doi.org/10.1086/306993)
- Wijnands, R., in't Zand, J. J. M., Rupen, M., et al. 2006, *A&A*, 449, 1117, doi: [10.1051/0004-6361:20054129](https://doi.org/10.1051/0004-6361:20054129)
- Wilms, J., Allen, A., & McCray, R. 2000, *ApJ*, 542, 914, doi: [10.1086/317016](https://doi.org/10.1086/317016)
- Winkler, C., Courvoisier, T. J. L., Di Cocco, G., et al. 2003, *A&A*, 411, L1, doi: [10.1051/0004-6361:20031288](https://doi.org/10.1051/0004-6361:20031288)
- Wood, K. S., Ray, P. S., Bandyopadhyay, R. M., et al. 2000, *ApJL*, 544, L45, doi: [10.1086/317287](https://doi.org/10.1086/317287)
- Yadav, J. S., Misra, R., Verdhhan Chauhan, J., et al. 2016, *ApJ*, 833, 27, doi: [10.3847/0004-637X/833/1/27](https://doi.org/10.3847/0004-637X/833/1/27)
- Yan, Z., & Yu, W. 2015, *ApJ*, 805, 87, doi: [10.1088/0004-637X/805/2/87](https://doi.org/10.1088/0004-637X/805/2/87)
- Yang, Z.-X., Zhang, L., Zhang, S.-N., et al. 2024, *ApJL*, 970, L33, doi: [10.3847/2041-8213/ad60bd](https://doi.org/10.3847/2041-8213/ad60bd)
- Yuan, F., & Narayan, R. 2014, *ARA&A*, 52, 529, doi: [10.1146/annurev-astro-082812-141003](https://doi.org/10.1146/annurev-astro-082812-141003)
- Yuan, W., Zhang, C., Chen, Y., & Ling, Z. 2022, in *Handbook of X-ray and Gamma-ray Astrophysics*, 86, doi: [10.1007/978-981-16-4544-0_151-1](https://doi.org/10.1007/978-981-16-4544-0_151-1)
- Yuan, W., Dai, L., Feng, H., et al. 2025, *Science China Physics, Mechanics, and Astronomy*, 68, doi: [10.1007/s11433-024-2600-3](https://doi.org/10.1007/s11433-024-2600-3)
- Yuan, X., Li, Z., Liu, X., et al. 2020, in *Society of Photo-Optical Instrumentation Engineers (SPIE) Conference Series*, Vol. 11445, *Ground-based and Airborne Telescopes VIII*, ed. H. K. Marshall, J. Spyromilio, & T. Usuda, 114457M, doi: [10.1117/12.2562334](https://doi.org/10.1117/12.2562334)
- Zdziarski, A. A., Johnson, W. N., & Magdziarz, P. 1996, *MNRAS*, 283, 193, doi: [10.1093/mnras/283.1.193](https://doi.org/10.1093/mnras/283.1.193)
- Zhang, B., Fan, Y. Z., Dyks, J., et al. 2006, *ApJ*, 642, 354, doi: [10.1086/500723](https://doi.org/10.1086/500723)
- Zhang, S.-N., Li, T., Lu, F., et al. 2020, *Science China Physics, Mechanics, and Astronomy*, 63, 249502, doi: [10.1007/s11433-019-1432-6](https://doi.org/10.1007/s11433-019-1432-6)
- Zhao, H.-S., Li, C.-K., Wang, J., et al. 2025, *Radiation Detection Technology and Methods*, doi: [10.1007/s41605-025-00526-8](https://doi.org/10.1007/s41605-025-00526-8)
- Życki, P. T., Done, C., & Smith, D. A. 1999, *MNRAS*, 309, 561, doi: [10.1046/j.1365-8711.1999.02885.x](https://doi.org/10.1046/j.1365-8711.1999.02885.x)